

ARTICLE

MRCK activates mouse oocyte myosin II for spindle rotation and male pronucleus centration

 Anne Bourdais¹ , Benoit Dehapiot¹ , and Guillaume Halet¹ 

Asymmetric meiotic divisions in oocytes rely on spindle positioning in close vicinity to the cortex. In metaphase II mouse oocytes, eccentric spindle positioning triggers cortical polarization, including the build-up of an actin cap surrounded by a ring of activated myosin II. While the role of the actin cap in promoting polar body formation is established, ring myosin II activation mechanisms and functions have remained elusive. Here, we show that ring myosin II activation requires myotonic dystrophy kinase-related Cdc42-binding kinase (MRCK), downstream of polarized Cdc42. MRCK inhibition resulted in spindle rotation defects during anaphase II, precluding polar body extrusion. Remarkably, disengagement of segregated chromatids from the anaphase spindle could rescue rotation. We further show that the MRCK/myosin II pathway is activated in the fertilization cone and is required for male pronucleus migration toward the center of the zygote. These findings provide novel insights into the mechanism of myosin II activation in oocytes and its role in orchestrating asymmetric division and pronucleus centration.

Introduction

In preparation for embryonic development, oocytes must haploidize their maternal genome. In mammalian oocytes, this is orchestrated through two meiotic divisions, leading to the formation of two small polar bodies in which extra chromosomes are discarded. To achieve these highly asymmetric divisions, oocytes position their meiotic spindle in close vicinity to the cortex, leading to cortical reorganization known as oocyte polarization (Chaigne et al., 2012; Yi et al., 2013; Mogessie et al., 2018). In ovulated mouse oocytes arrested at metaphase II (MII), a classical feature of cortical polarization is the establishment of a thick actin cap delineated by a stationary ring of activated nonmuscle myosin II, thereby defining the polar body-forming region (Maro et al., 1984; Longo and Chen, 1985; Van Blerkom and Bell, 1986; Deng et al., 2007; Wang et al., 2011). Remarkably, mouse oocyte polarization exemplifies a nongenetic function of DNA, whereby cortical reorganization is driven from a distance via a cytoplasmic gradient of activated Ran GTPase generated by maternal chromosomes (Deng et al., 2007; Yi et al., 2011; Dehapiot and Halet, 2013; Wang et al., 2020; Mori et al., 2021). Accordingly, the polarity pathway is conserved during anaphase II, with the establishment of two smaller actin caps, each surrounded by a ring of myosin II, in the cortical protrusions overlying segregated chromatids (Wang et al., 2020; Dehapiot et al., 2021).

In an effort to describe further the molecular cascade for cortical polarization, we and others previously identified the small GTPase Cdc42 as a key intermediate in the formation of the actin cap (Dehapiot et al., 2013; Dehapiot and Halet, 2013; Wang et al., 2013). As a likely downstream effector of Cdc42, the Arp2/3 complex is enriched in the polarized cortex and promotes the assembly of the actin cap, suggesting that the latter is organized as a branched network (Pollard, 2007; Yi et al., 2011; Zhang et al., 2017; Bourdais et al., 2021). Through the use of diverse inhibitors and molecular tools, the role of the actin cap in promoting polar body formation was demonstrated (Maro et al., 1984; Schatten et al., 1986; Terada et al., 2000; Dehapiot et al., 2013; Wang et al., 2013). In addition, Arp2/3 inhibition was shown to induce MII spindle drifting away from its eccentric position due to reversed cytoplasmic streaming powered by myosin II (Yi et al., 2011). These findings point to a functional crosstalk between actin and myosin II cytoskeletal assemblies at the polarized cortex. However, the mechanism underlying ring myosin II activation and its role during oocyte meiotic divisions remain unclear. Intriguingly, we recently uncovered that the active myosin II ring is lost upon Cdc42 inactivation (Dehapiot et al., 2021). Therefore, while the current view is that the myosin II ring is driven by myosin light chain kinase (MLCK; Deng et al.,

¹University of Rennes, CNRS - UMR 6290, Institute of Genetics and Development of Rennes, Rennes, France.

Correspondence to Guillaume Halet: guillaume.halet@univ-rennes1.fr

B. Dehapiot's current affiliation is ScopeM, ETH Zurich, Zurich, Switzerland.

© 2023 Bourdais et al. This article is distributed under the terms of an Attribution-Noncommercial-Share Alike-No Mirror Sites license for the first six months after the publication date (see <http://www.rupress.org/terms/>). After six months it is available under a Creative Commons License (Attribution-Noncommercial-Share Alike 4.0 International license, as described at <https://creativecommons.org/licenses/by-nc-sa/4.0/>).

2005, 2007; Matson et al., 2006; Ajduk et al., 2011; McGinnis et al., 2015; Mackenzie et al., 2016), our observations rather support a Cdc42-dependent mechanism. In line with this view, we previously reported that Cdc42-inhibited MII oocytes do not experience spindle drift, despite a loss of the actin cap (Dehapiot et al., 2013; Dehapiot and Halet, 2013).

Fertilization triggers the resumption of meiosis II, leading to sister chromatid separation, emission of the second polar body (PB2), and ultimately, meiotic exit and formation of the maternal and paternal haploid pronuclei (Clift and Schuh, 2013). During the early stages of anaphase II, the spindle remains parallel to the cortex, then reorients perpendicularly in a process referred to as spindle rotation, allowing for internalization of one cluster of chromatids, while the other is discarded into the PB2 (Maro et al., 1984; Zhu et al., 2003). Significant advances were recently made in our understanding of spindle rotation, which was shown to entail spontaneous symmetry breaking in cortical polarization signals, with unilateral furrow ingression serving as a driving force (Wang et al., 2020; Dehapiot et al., 2021). While actomyosin contractility as a whole is critical to PB2 formation and cytokinesis, the specific contribution of ring myosin II could not be firmly established due to the lack of discriminating tools.

To gain insight into ring myosin II activation and function, we explored further the upstream regulation by Cdc42. We show that ring myosin II requires the polarized activation of myotonic dystrophy kinase-related Cdc42-binding kinase β (MRCK β ; also known as Cdc42bpb), downstream of Cdc42 activation (Cdc42-GTP). The MRCK/myosin II pathway is conserved during anaphase II and drives ring myosin II activation in the cortical protrusions overlying segregated chromatids. MRCK inhibition resulted in a complete loss of ring myosin II, while cytokinetic myosin II activation in the cleavage furrow was preserved, owing to spatially segregated Cdc42 and RhoA zones. The loss of ring myosin II was associated with spindle rotation defects during anaphase II, leading to spindle distortion and a failure of PB2 cytokinesis. Strikingly, a subset of MRCK-inhibited oocytes eventually achieved symmetry breaking through disengaging one cluster of chromatids from the anaphase II spindle, thus enabling rotation to proceed. In addition, we show that in fertilized oocytes, a similar Cdc42/MRCK/myosin II module sequentially promotes outward bulging and later flattening of the fertilization cone (FC) for inward migration of the male PN.

Results

Polarized myosin II activation relies on Cdc42 signaling

To explore the role of Cdc42 in the establishment of the myosin II ring, MII oocytes were treated with the allosteric Cdc42 inhibitor ML-141 (Hong et al., 2013) and examined for MRLC phosphorylation at Ser19 (P-MRLC) as a proxy for myosin II activation (Vicente-Manzanares et al., 2009; Heissler and Sellers, 2016). In control oocytes treated with vehicle (DMSO), P-MRLC showed the landmark ring accumulation at the rim of the F-actin cap (Fig. 1 A). In contrast, treatment with ML-141 (5 μ M, 1 h) induced a complete loss of the P-MRLC ring (Fig. 1, A and F), thus recapitulating our previous observations with

Cdc42T17N expression (Dehapiot et al., 2021). Cdc42 inhibition was also invariably associated with a partial or complete loss of the polarized F-actin cap (Fig. 1 A, white arrow), consistent with Cdc42 acting as a key intermediate in chromatin-induced F-actin polarization. Transcriptome and translatome profiling studies reported the expression of the two predominant myosin II heavy chain paralogs, myosin IIA and IIB, in mouse MII oocytes, while myosin IIC was not detected (Tang et al., 2009; Hu et al., 2022). Accordingly, myosin IIA distributed as a polarized ring in the cortex of MII oocytes, while myosin IIB was not detected at that stage (Fig. S1, A and B). Treatment with ML-141 resulted in a similar loss of the polarized myosin IIA ring (Fig. S1 A), consistent with a disassembly of myosin II filaments consecutive to MRLC dephosphorylation.

Based on the use of compound ML-7, previous studies have argued that the myosin II ring was driven by MLCK, a kinase primarily activated by Ca^{2+} /calmodulin (Hong et al., 2011). However, we could not achieve significant myosin II inhibition using 15 μ M ML-7 (Fig. S2, A–C). To clarify further the contribution of MLCK, we employed three alternative inhibitory strategies: (1) Ca^{2+} depletion (Miao et al., 2012), (2) injection of peptide-18 (Lukas et al., 1999), and (3) treatment with 1 μ M wortmannin, a potent and irreversible MLCK inhibitor (Nakanishi et al., 1992; Davies et al., 2000). However, none of these treatments demonstrated any inhibitory effect on the P-MRLC ring (Fig. S2, A–C), arguing strongly against MLCK as the MRLC kinase.

Another two classic MRLC kinases are Rho-associated coiled-coil containing protein kinase (ROCK) and group I p21-activated kinases (PAKs), which act downstream of RhoA and Cdc42/Rac, respectively (Amano et al., 1996; Chew et al., 1998; Wilkinson et al., 2005). A role for ROCK appears highly unlikely since RhoA and ROCK are absent from the polarized cortex, and the P-MRLC ring is resistant to ROCK inhibition (Dehapiot et al., 2021). Likewise, IPA-3, an allosteric inhibitor of group I PAKs (Deacon et al., 2008), did not prevent polarized myosin II activation (Fig. S2, A–C). Collectively, these data suggest that polarized myosin II localization and activation in MII oocytes involve an MRLC kinase acting downstream of Cdc42, other than PAK.

Cdc42 recruits MRCK β to the polarized cortex for myosin II activation

MRCK is a conserved serine/threonine kinase that promotes myosin II activation directly via MRLC Ser19 phosphorylation (Leung et al., 1998; Tan et al., 2011). Owing to a canonical Cdc42/Rac interactive binding (CRIB) domain located at its C terminus (Fig. S3 A), MRCK is targeted to sites of Cdc42 activation, making it a valuable candidate for polarized myosin II activation (Ando et al., 2013; Unbekandt and Olson, 2014; Zhao and Manser, 2015). Consistent with this idea, MRCK β was detected in the polarized cortex of MII oocytes (Fig. 1, B and C). Consistent with Cdc42 acting as a polarizing cue, treatment with ML-141 inhibited the cortical localization of MRCK β (Fig. 1, B and C). Similarly, an MRCK β -EGFP construct (Ando et al., 2013) decorated the polarized cortex, while a mutant MRCK β impaired for Cdc42-GTP binding (MRCK β H1593/I596A; Leung et al., 1998; Ando et al., 2013) remained cytosolic (Fig. 1 D and Fig. S3 B).

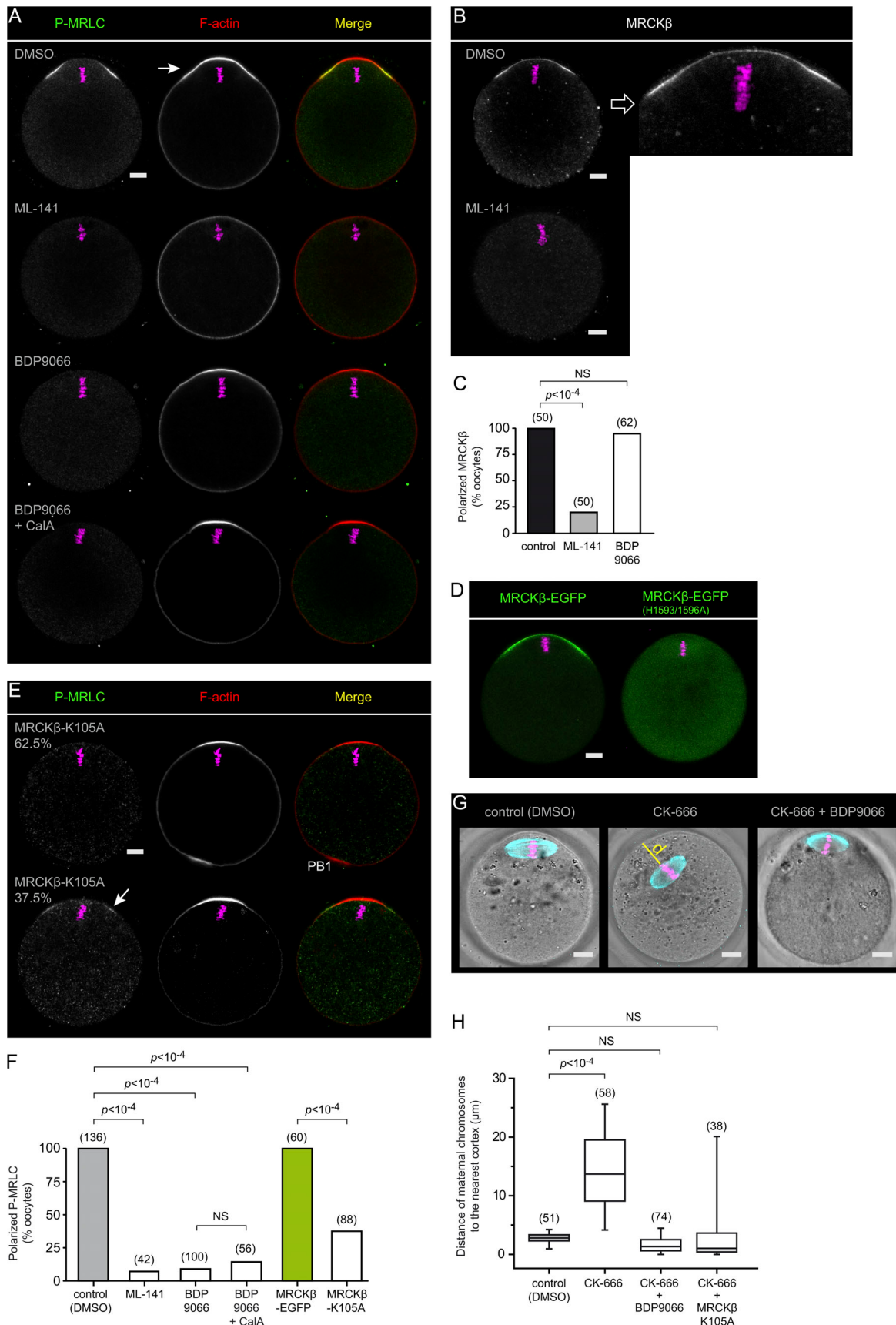


Figure 1. MRCK promotes myosin II activation in the polarized cortex. **(A)** Immunofluorescence detection of activated myosin II (P-MRLC) in MII oocytes treated for 1 h with DMSO, ML-141 (5 μ M), BDP9066 (1 μ M), or a combination of BDP9066 (1 μ M) and calyculin A (CalA; 0.5 nM). Images are single confocal

frames taken across metaphase chromosomes. **(B)** Immunofluorescence detection of endogenous MRCK β in MII oocytes. The top row shows a control oocyte treated with DMSO. An enlarged view of the polarized cortex is shown on the right. The bottom row shows an oocyte treated with ML-141 (5 μ M). **(C)** Bar graph depicting the fraction of oocytes showing polarized accumulation of MRCK β in MII oocytes treated with DMSO, ML-141, or BDP9066. P values were calculated using Fisher's exact test. **(D)** Localization of MRCK β -EGFP (left) and MRCK β H1593/1596A-EGFP (right) in live MII oocytes. Note the absence of cortical localization for the Cdc42 binding-deficient MRCK β . Images are representative of >40 similar observations. **(E)** Immunofluorescence detection of activated myosin II (P-MRLC) in MII oocytes expressing MRCK β -K105A. A majority of oocytes (62.5%) showed a complete loss of the P-MRLC ring (top row), while the remaining oocytes (37.5%) showed incomplete inhibition (bottom row; white arrow). **(F)** Bar graph depicting the percentage of MII oocytes showing a P-MRLC ring in various experimental conditions as shown in A, D, and E. P values were calculated using Fisher's exact test. **(G)** Immunofluorescence detection of tubulin showing spindle localization in MII oocytes treated with DMSO (left), CK-666 (100 μ M) for 3 h (middle), and CK-666 (100 μ M) and BDP9066 (1 μ M) for 3 h (right). The yellow line shows the distance (d) separating the maternal chromosomes from the nearest cortex. **(H)** Box plot showing the distance between maternal chromosomes and the nearest cortical region in oocytes treated with DMSO (controls), CK-666 alone, CK-666 and BDP9066, as illustrated in G, and in oocytes expressing MRCK β -K105A treated with CK-666. P values were calculated using two-tailed Student's *t* test. F-actin was labeled with Alexa Fluor 568-phalloidin. Chromosomes were stained with TO-PRO-3 (A, B, E, and G; magenta) or with SiR-DNA (D; magenta). The number of oocytes scored is indicated above each bar/box (C, F, and H). Scale bars are 10 μ m. In A, D, and E, scale bars apply to the entire panel. NS: nonsignificant.

We next examined the contribution of MRCK to the polarized activation of myosin II. Because genetic ablation of MRCK was reported to substantially rewire kinase signaling and potentially impede kinase-independent functions (Kurimchak et al., 2020), we first aimed for a dominant-negative approach (Leung et al., 1998; Nakamura et al., 2000; Tan et al., 2008). Thus, a kinase-dead MRCK β mutant was generated by substituting lysine 105 in the kinase domain for alanine (K105A; Unbekandt et al., 2020). Accordingly, expression of MRCK β -K105A via cRNA injection abolished the P-MRLC ring in a majority (62.5%) of oocytes, while the expression of MRCK β -EGFP had no effect (Fig. 1, E and F). The remaining oocytes (37.5%) showed residual P-MRLC signal (Fig. 1, E and F), likely reflecting lower expression of the kinase-dead mutant. Alternatively, we challenged oocytes with the recently characterized small molecule inhibitor BDP9066, which is highly selective for MRCK, while having no effect on MLCK (Unbekandt et al., 2018). Remarkably, acute MRCK inhibition with BDP9066 (1 μ M, 1 h) abolished MRLC phosphorylation in virtually all oocytes examined (Fig. 1, A and F). The myosin IIA ring was lost accordingly, consistent with disassembly of the actomyosin filaments (Fig. S1 A). In addition, we noticed that inhibition of ring myosin II was associated with oocyte rounding through the loss of the outward bulge that otherwise defines the amicrovillar polarized cortex (Fig. 1 A). Hence, acute exposure to BDP9066 induced a gradual flattening of the bulge, while the MII spindle remained stationary (Video 1).

MRCK may also activate myosin II indirectly by the phosphorylation of the protein phosphatase 1 regulatory subunit MYPT1, leading to inactivation of myosin phosphatase activity (Tan et al., 2001; Wilkinson et al., 2005). However, supplementation of the culture medium with calyculin A, a potent phosphatase 1 inhibitor (Ishihara et al., 1989), did not rescue ring P-MRLC in MRCK-inhibited oocytes (Fig. 1, A and F). While this observation does not rule out MYPT1 as an additional substrate, it supports the view that oocyte MRCK acts directly as the MRLC Ser19 kinase.

To establish the functional inhibition of ring myosin II in MRCK-inhibited oocytes, we employed CK-666 to inhibit the Arp2/3 complex and induce MII spindle drift powered by myosin II contractility (Nolen et al., 2009; Yi et al., 2011). Thus, oocytes treated with CK-666 (100 μ M; 3 h) alone demonstrated a substantial drift of the spindle toward the cell interior (Fig. 1, G

and H). In contrast, the spindle remained closely apposed to the cortex in oocytes treated with both CK-666 and BDP9066 and in MRCK β -K105A-expressing oocytes treated with CK-666 (Fig. 1, G and H). These results are consistent with a loss of actomyosin contractility in the polarized cortex of MRCK-inhibited oocytes. Importantly, these data also demonstrate that inactivation of ring myosin II is not associated with a drift of the MII spindle away from the cortex, contrary to previous studies using ML-7 (Deng et al., 2005, 2007; McGinnis et al., 2015). Collectively, the above data indicate that Cdc42 activation acts as a spatial cue for MRCK recruitment at the polarized cortex, leading to MRLC phosphorylation and establishment of the active myosin II ring. Contractility of the ring provides tension forces resulting in the outward bulging of the actin-rich polarized cortex.

Crosstalk between ring myosin II and the Arp2/3 complex shapes the polarized cortex

Ring myosin II and the Arp2/3 complex were recently suggested to engage in a mutual inhibition at the polarized cortex, whereby myosin would restrict the size of the actin cap (Wang et al., 2020). However, this conclusion was reached via artificial activation of Rho at the cortex, which may antagonize Cdc42 signaling (Vaughan et al., 2011). We performed MRCK inhibition to ask directly whether ring myosin II opposes Arp2/3. Contrary to this expectation, MRCK-inhibited oocytes showed a significant reduction of the size of the actin cap, though we never observed a complete loss of the cap (Fig. 2, A and B). Interestingly, we uncovered that the outer region of the polarized Arp2/3 domain overlaps with ring myosin II (Fig. 2 C, white arrows). Moreover, MRCK inhibition resulted in a loss of the outer region of the Arp2/3 cap, matching the loss of the P-MRLC ring (Fig. 2, C and D). These data reveal an unanticipated role of ring myosin II in the broadening of the polarized Arp2/3 domain, and hence the actin cap. In contrast, the Arp2/3 domain was completely lost after treatment with ML-141 (Fig. 2, C and D), consistent with Cdc42 acting as a polarizing cue for the recruitment and activation of the F-actin cap nucleation machinery (Dehapiot et al., 2013; Wang et al., 2013).

MRCK β demonstrated comparable accumulation at the rim of the F-actin cap, matching the P-MRLC ring (Fig. 3, A-C). This ring enrichment was unaffected by myosin II inhibition (Fig. 3 C), ruling out a convergent advection mechanism driven by actomyosin contractility (Kuo et al., 2011; Munjal et al., 2015).

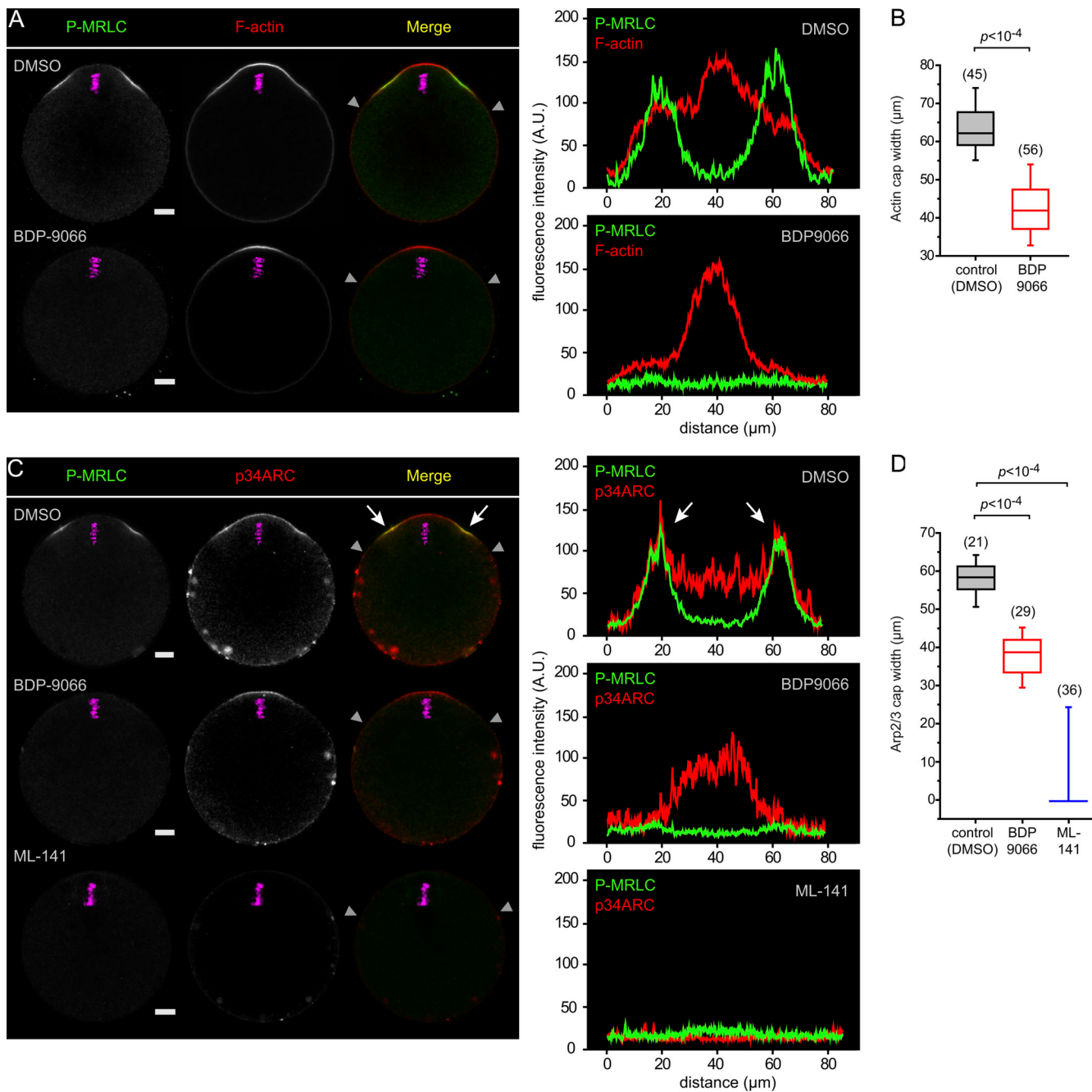


Figure 2. Ring myosin II broadens the polarized actin cap and Arp2/3 complex domain. **(A)** Immunofluorescence detection of activated myosin II (P-MRLC) in MII oocytes treated for 1 h with DMSO (top row) or BDP9066 (1 μM; bottom row). F-actin was labeled with Alexa Fluor 568-phalloidin. **(B)** Box plot showing the width of the actin cap in control MII oocytes treated with DMSO and in MII oocytes treated with BDP9066 (1 μM). P value was calculated using two-tailed Student's *t* test. The number of oocytes scored is indicated above each box. **(C)** Immunofluorescence detection of activated myosin II (P-MRLC) and the Arp2/3 complex (p34ARC) in MII oocytes treated for 1 h with DMSO (top row), BDP9066 (1 μM; middle row), or ML-141 (5 μM; bottom row). White arrows point to the colocalization of P-MRLC and p34ARC at the shoulders of the actin cap. **(D)** Box plot showing the width of the Arp2/3 cap in control MII oocytes treated with DMSO and in MII oocytes treated with BDP9066 (1 μM) or ML-141 (5 μM). P values were calculated using two-tailed Student's *t* test. The number of oocytes scored is indicated above each box. Chromosomes were stained with TO-PRO-3 (magenta). Scale bars are 10 μm. In A and C, fluorescence intensity profiles are shown corresponding to the polarized cortex region delineated by the two gray arrowheads in the merged image.

We therefore asked whether the anchoring GTPase Cdc42 was also enriched as a ring. To test this idea, we designed a Cdc42-GTP biosensor derived from the minimal Cdc42-GTP-binding fragment of human MRCKβ that we referred to as MRCK-derived Cdc42-GTP biosensor (MCB; Fig. S3, A and B).

Indeed, MCB-EGFP decorated the polarized cortex of MII oocytes and was released to the cytosol upon treatment with ML-141 (Fig. S3, C and D). Likewise, substitution of the two critical histidine residues in the CRIB domain for alanine (H1593/1596A; Leung et al., 1998; Ando et al., 2013) abolished cortical localization (Fig.

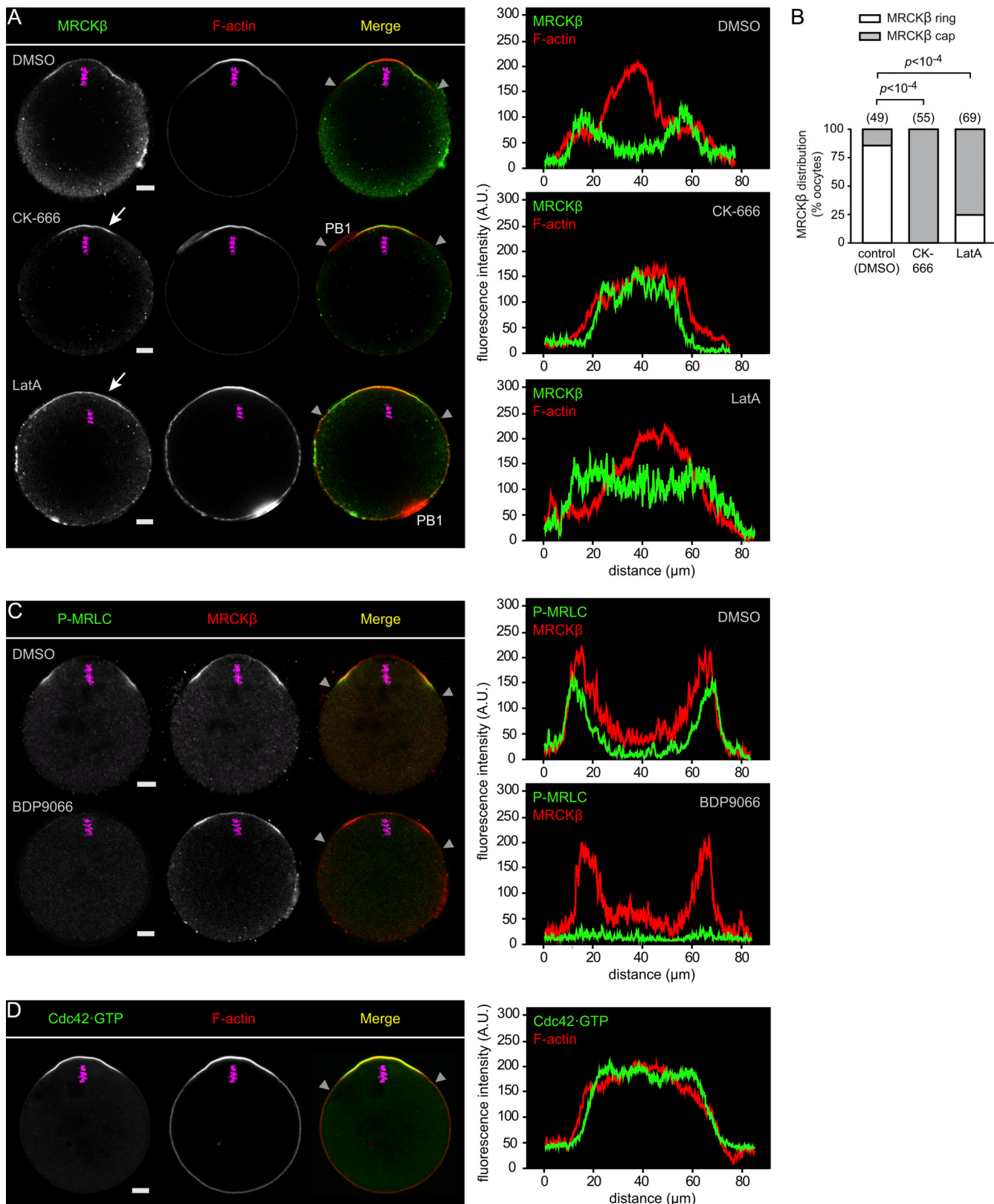


Figure 3. Actin dynamics shape MRCK β ring distribution in the polarized cortex. **(A)** Immunofluorescence detection of MRCK β in MII oocytes treated with DMSO (top), CK-666 (100 μ M, 3 h; middle), or Latrunculin A (LatA; 0.5 μ M, 10 min; bottom). Arrows point to MRCK β redistributed as a polarized cap. **(B)** Bar graph depicting the fraction of MII oocytes (%) showing MRCK β distributed as a ring or as a cap, as shown in A. Oocytes were treated with DMSO (control), CK-666, or Latrunculin A (LatA), as shown in A. Oocytes in which the MII spindle had relocated to the center after CK-666 treatment, resulting in a complete loss of polarized MRCK β , were not considered for analysis. P values were calculated using Fisher's exact test. The number of oocytes scored is indicated above each bar. **(C)** Immunofluorescence detection of phospho-MRLC (P-MRLC) and MRCK β in MII oocytes treated with DMSO (top) or BDP9066 (100 μ M, 3 h; middle). Arrows point to polarized P-MRLC/MRCK β distribution. **(D)** Immunofluorescence detection of Cdc42-GTP and F-actin in oocytes. Arrows point to polarized Cdc42-GTP/F-actin distribution. Scale bars: 10 μ m.

bar. **(C)** Immunofluorescence detection of activated myosin II (P-MRLC) and MRCK β in MII oocytes treated for 1 h with DMSO (top) or BDP9066 (1 μ M; bottom). **(D)** Detection of Cdc42-GTP in an MII oocyte expressing the biosensor MCB-EGFP. Fluorescence intensity profiles correspond to the polarized cortex region delineated by the two gray arrowheads in the merged images. F-actin was labeled with Alexa Fluor 568-phalloidin. Chromosomes were stained with TO-PRO-3 (magenta). Scale bars are 10 μ m. PB1: first polar body.

S3, B and E). Fluorescence profile analysis revealed that the Cdc42-GTP signal was maximal in the central region of the polarized cortex and faded gradually with increasing distance, much similar to the F-actin cap signal (**Fig. 3 D**). While this pattern likely reflects upstream regulation by the Ran-GTP gradient ([Deng et al., 2007](#)), it is inconsistent with MRCK β clustering as a ring. In contrast, short treatment with CK-666 (100 μ M, 1 h) to inactivate the Arp2/3 complex resulted in a redistribution of MRCK β into a polarized cap (**Fig. 3, A and B**), as was previously described for ring myosin II ([Yi et al., 2011](#)). Interestingly, spindle drift was not yet observable at this stage and the bulk of the actin cap was preserved, consistent with the fact that CK-666 does not disassemble preformed branches ([Herrick et al., 2013](#)). In addition, a fairly short treatment with Latrunculin A (0.5 μ M, 10 min), an actin polymerization inhibitor that was previously shown to abolish cortical actin flow in oocytes ([Coué et al., 1987; Yi et al., 2011](#)), also resulted in MRCK β redistributing as a polarized cap (**Fig. 3, A and B**). These data suggest that the ring pattern of the MRCK/myosin II module is driven by Arp2/3 activation in the polarized cortex, but may be unrelated to the build-up of the actin cap itself. Rather, the circumferential actin flow powered by polarized Arp2/3-dependent F-actin nucleation may transport MRCK/myosin II for clustering at the rim of the actin cap, analogous to actin flow-mediated myosin IIA partitioning in polarized fibroblasts and motile epithelial cells ([Yi et al., 2011; Lomakin et al., 2015; Beach et al., 2017](#)).

Cdc42 and RhoA zones define two cortical myosin II pools in anaphase II

We recently uncovered that upon oocyte activation, the P-MRLC ring splits into two smaller rings overlying the two clusters of segregated chromatids, while a second pool of myosin II is activated de novo by the RhoA/ROCK pathway to drive unilateral membrane furrowing above the central spindle ([Dehapiot et al., 2021; Fig. 4, E and F](#)). We, therefore, inferred that the Cdc42/MRCK pathway remains active in anaphase II, yet spatially segregated from the RhoA/ROCK pathway. To substantiate this view, we examined the spatial distribution of activated Cdc42 and RhoA GTPases and their cognate effector kinases. In live MII oocytes, Cdc42-GTP was readily detected in the polarized cortex, while RhoA activation, monitored using the mCherry-AHPH biosensor ([Piekny and Glotzer, 2008](#)), remained undetectable (**Fig. 4 A**). Upon activation with SrCl₂ to trigger cell cycle progression to anaphase II, the Cdc42-GTP cap split into two smaller caps associated with each of the two chromatid clusters, while the intervening cortical region showed RhoA-GTP accumulation (**Fig. 4 A**). Accordingly, MRCK β localized selectively in the two cortical protrusions overlying maternal chromatids, while ROCK1 concentrated in a narrow region over the central spindle (**Fig. 4, B and C**). Myosin IIA was detected both in the rings and

in the ingressing furrow (**Fig. S1 C**), in line with previous observations ([Sharif et al., 2015](#)). Of note, myosin IIB became detectable at the cortex of anaphase II oocytes and concentrated exclusively in the cytokinetic furrow (**Fig. S1 D**). Consistent with our observations in MII oocytes, MRCK β colocalized precisely with the two smaller P-MRLC rings but not with cytokinetic P-MRLC in the cleavage furrow (**Fig. 4 D**). Accordingly, MRCK inhibition resulted in the selective loss of ring P-MRLC, while cytokinetic P-MRLC was preserved (**Fig. 4, E and F**). Furthermore, simultaneous treatment with MRCK (BDP9066) and ROCK (Y-27632) inhibitors resulted in a complete loss of cortical myosin II activation (**Fig. 4, E and F**).

Together with our previous findings on the activation of the RhoA/ROCK pathway during anaphase II ([Dehapiot et al., 2021](#)), the above data provide strong evidence for the coexistence of two distinct myosin II populations in the cortex of activated oocytes, downstream of spatially segregated Cdc42/MRCK and RhoA/ROCK pathways. While the role of the ROCK/myosin II module in driving cytokinetic furrow ingression has been demonstrated, the role of ring myosin II during anaphase II has remained elusive ([Wang et al., 2020; Dehapiot et al., 2021](#)). We, therefore, performed MRCK inhibition with BDP9066 to clarify the role of ring myosin II in activated oocytes.

MRCK promotes spindle rotation during anaphase II

To find out what role ring myosin II might play during anaphase II, we performed live imaging of spindle and chromosome dynamics in SrCl₂-activated oocytes. As previously reported ([Maro et al., 1984; Wang et al., 2020; Dehapiot et al., 2021](#)), vehicle (DMSO)-treated control oocytes initiated anaphase II in a symmetrical fashion, whereby the anaphase II spindle lay parallel to the cortex, leading to the bulging of two membrane protrusions over each set of segregated chromatids (**Fig. 5 A and Video 2**). This configuration was short-lived, however, as unilateral furrowing above the spindle equator was quickly followed by spindle rotation, culminating in the extrusion of the PB2, while a single haploid set of maternal chromosomes was retained in the oocyte (**Fig. 5, A and D**; and [Video 2](#)). During the course of rotation, the internalized cluster of chromatids remained firmly connected to the anaphase spindle and was thus relocated deeper into the inner cytoplasm, while the overlying cortical protrusion resolved. Accordingly, upon meiotic exit, a single female pronucleus (PN) formed in the oocyte cytoplasm at a distance from the cortex (**Fig. 5, E and F**).

Oocytes treated with the MRCK inhibitor BDP9066 initiated anaphase II in the same fashion as controls (**Fig. 5, B and C**). However, while a small fraction of these oocytes achieved symmetry breaking to form the PB2 (**Fig. 5 D**), the remaining oocytes exhibited striking spindle rotation defects. In about half of these oocytes, the anaphase spindle failed to rotate and both chromatid clusters remained closely apposed to the overlying

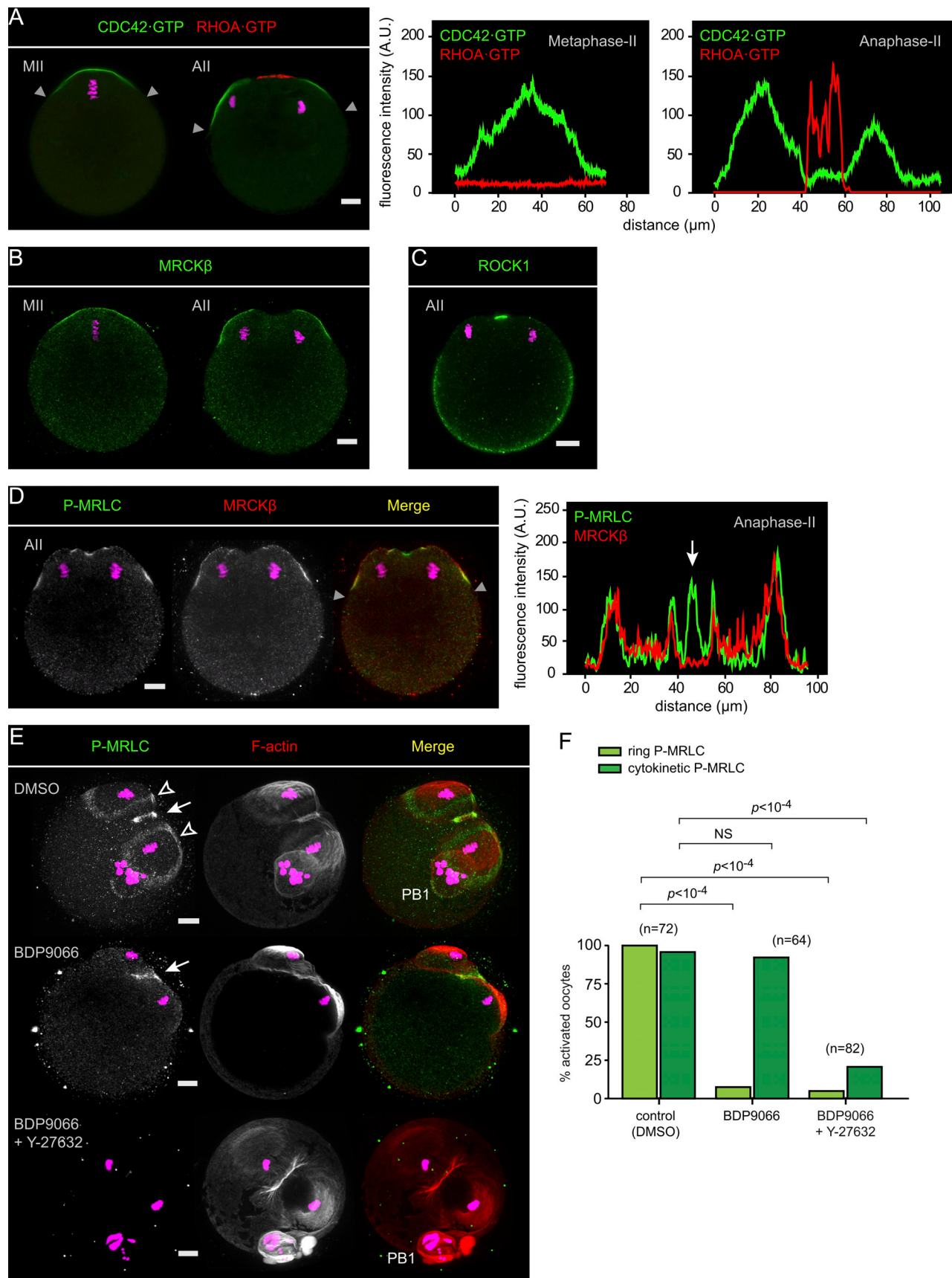


Figure 4. Two distinct myosin II pools coexist in the cortex of activated oocytes. **(A)** Detection of Cdc42-GTP (green) and RhoA-GTP (red) in live oocytes at the MII (left) and anaphase II (All, right) stages. Oocytes were injected at the MII stage with cRNAs encoding the MCB-EGFP and mCherry-AHPH biosensors.

Images are z-compressions of three consecutive confocal frames. **(B)** Immunofluorescence detection of MRCK β in fixed MII (left) and All (right) oocytes. **(C)** Immunofluorescence detection of ROCK1 in an All oocyte. **(D)** Immunofluorescence detection of activated myosin II (P-MRLC) and MRCK β in an All oocyte. **(E)** Immunofluorescence detection of activated myosin II (P-MRLC) in the cortex of activated oocytes undergoing All. Oocytes were treated with DMSO (top row), BDP9066 (1 μ M; middle row), or a combination of BDP9066 and Y-27632 (respectively 1 and 50 μ M; bottom row). Open arrowheads point to the P-MRLC rings overlying the chromatid clusters in the control (DMSO) oocyte. White arrows point to cytokinetic P-MRLC in the control (DMSO) and BDP9066-treated oocytes. Images are z-compressions of 33 (DMSO), 15 (BDP9066), and 30 (BDP9066 + Y-27632) consecutive confocal frames. **(F)** Bar graph depicting the percentage of activated oocytes showing ring myosin II activation (ring P-MRLC, light green) and/or cytokinetic myosin II activation (cytokinetic P-MRLC, dark green). Oocytes were treated with DMSO, BDP9066, or a combination of BDP9066 and Y-27632, as shown in E. P values were calculated using Fisher's exact test. NS: not significant. The number of oocytes scored is indicated in parentheses. F-actin was labeled with Alexa Fluor 568-phalloidin. Chromosomes were stained with SiR-DNA (A) or TO-PRO-3 (B-E). Fluorescence intensity profiles in A and D correspond to the cortical regions delineated by the gray arrowheads in the merge images. In D, the white arrow points to the ingressing furrow region that is enriched in P-MRLC but devoid of MRCK β . PB1: first polar body. Scale bars are 10 μ m. In A and B, scale bars apply to the entire panel.

cortex during furrow ingression (Fig. 5 B and Video 3). As a result, the anaphase II spindle experienced severe distortion while the furrow ingressed further, as neither of the two chromatid clusters would let go of cortical anchoring. Eventually, two polar body-like protrusions were formed, each containing one set of chromatids at the poles of a distorted spindle (Fig. 5, B and D; and Video 3). The distorted spindle configuration persisted until meiotic exit, leading to the formation of binucleate parthenotes (Fig. 5, E and F). In the remaining MRCK-inhibited oocytes, we observed a striking breakage of the anaphase II spindle, whereby one of the cortically anchored chromatin clusters disengaged from the spindle pole at the onset of cortical ingression (Fig. 5, C and D; and Video 4). As furrowing progressed further, spindle rotation occurred in a consistent fashion, with the chromatin-associated spindle pole forming the PB2 and the chromatin-less spindle pole reorienting toward the cell interior (Fig. 5 C and Video 4). The detached cluster remained in close vicinity of the overlying cortex; hence the PN that formed at meiotic exit was often still enclosed in a polar body-like protrusion (Fig. 5 E, arrow). Similar spindle rotation defects, including broken spindle figures, were observed in activated oocytes expressing dominant-negative MRCK β -K105A (Fig. 5, G and H; and Video 5). The rate of spindle rotation defects in these oocytes was, however, <50% (Fig. 5 H), likely due to residual endogenous MRCK activity (see Fig. 1, E and F).

We next examined the effect of MRCK inhibition during fertilization. Cumulus-oocyte complexes were placed in HTF (human tubal fluid) medium and inseminated with capacitated sperm in the presence of DMSO or BDP9066 (2 μ M). Zygotes were fixed 6.5 h after insemination and scored for polar body emission and PN formation. Immuno-detection of H3K4me3 was performed to unambiguously discriminate the female PN (H3K4me3 positive) from the male PN (Fig. 5 I; Lepikhov and Walter, 2004). Intriguingly, we observed defects in male PN centration in MRCK-inhibited oocytes (see below). In addition, MRCK inhibition was associated with defects in PB2 emission, as evidenced by the presence in the cytoplasm of two maternal pronuclei (Fig. 5, J and K). The binucleation phenotype was however less pronounced than in SrCl₂-activated oocytes (Fig. 5, F and K), possibly due to the presence in the HTF medium of a fairly high amount of BSA (4 mg/ml), which we found to interfere with BDP9066 efficiency (see Materials and methods).

Collectively, the above results suggest that activation of the Cdc42/MRCK pathway in the cortex overlying segregated

chromatids is required for normal spindle rotation during anaphase II. Spindle rotation defects in MRCK-inhibited oocytes appear to lie in the inability of chromatid clusters to let go of their cortical anchoring. However, chromatid disengagement at one pole of the anaphase spindle can allow for immediate rescue of spindle rotation.

MRCK promotes myosin II activation in the FC and centration of the male PN

Shortly after sperm fusion with the oocyte, the so-called fertilization cone (FC) is formed at the site of sperm entry. The general features of the FC are reminiscent of the polarized cortex overlying the MII spindle, i.e., an amicropillar membrane protrusion enriched in F-actin and myosin II, whose formation requires nearby chromatin signaling (Maro et al., 1984; Simerly et al., 1998; Deng et al., 2005; Deng and Li, 2009; Ajduk et al., 2011). In the same line, we observed that active myosin II (P-MRLC) localized as a ring at the boundary of the FC (Fig. 6, A and B; and Fig. S4 A), akin to the P-MRLC ring overlying maternal chromosomes. In addition, activated myosin II similarly overlapped with the rim of the FC actin cap (Fig. 6 A). We, therefore, surmised that MRCK may similarly regulate myosin II activation in the FC. Consistent with this idea, the FC was enriched in Cdc42-GTP (Fig. S4 B), and MRCK β accumulated as a ring at the boundary of the FC, matching the P-MRLC ring (Fig. S4, C and D). Significantly, supplementation of the fertilization medium with BDP9066 (2 μ M) abolished the FC P-MRLC ring (Fig. 6, A and B). Interestingly, using average cortical curvature as a proxy for protrusion, the MRCK inhibitor was also found to prevent the outward bulging of the FC (Fig. 6, A and C). These data suggest that myosin II activation in the FC also relies on the Cdc42/MRCK pathway and orchestrates FC protrusion.

Previous studies have demonstrated that FC outward protrusion is not a prerequisite for successful sperm fusion and oocyte activation (Maro et al., 1984; Schatten et al., 1986; Terada et al., 2000). However, a recent study suggested that the flattening of the FC shortly after PB2 emission initiates the migration of the male PN toward the center of the zygote for apposition with the female PN ahead of the first embryonic cleavage (Scheffler et al., 2021). To investigate any defect in male PN migration, oocytes were fertilized in vitro and zygotes showing a PB2 were further cultured in the presence of DMSO (control) or BDP9066 (Fig. 6 D). Zygotes were fixed 8 h after insemination, at which time the pronuclei are expected to have

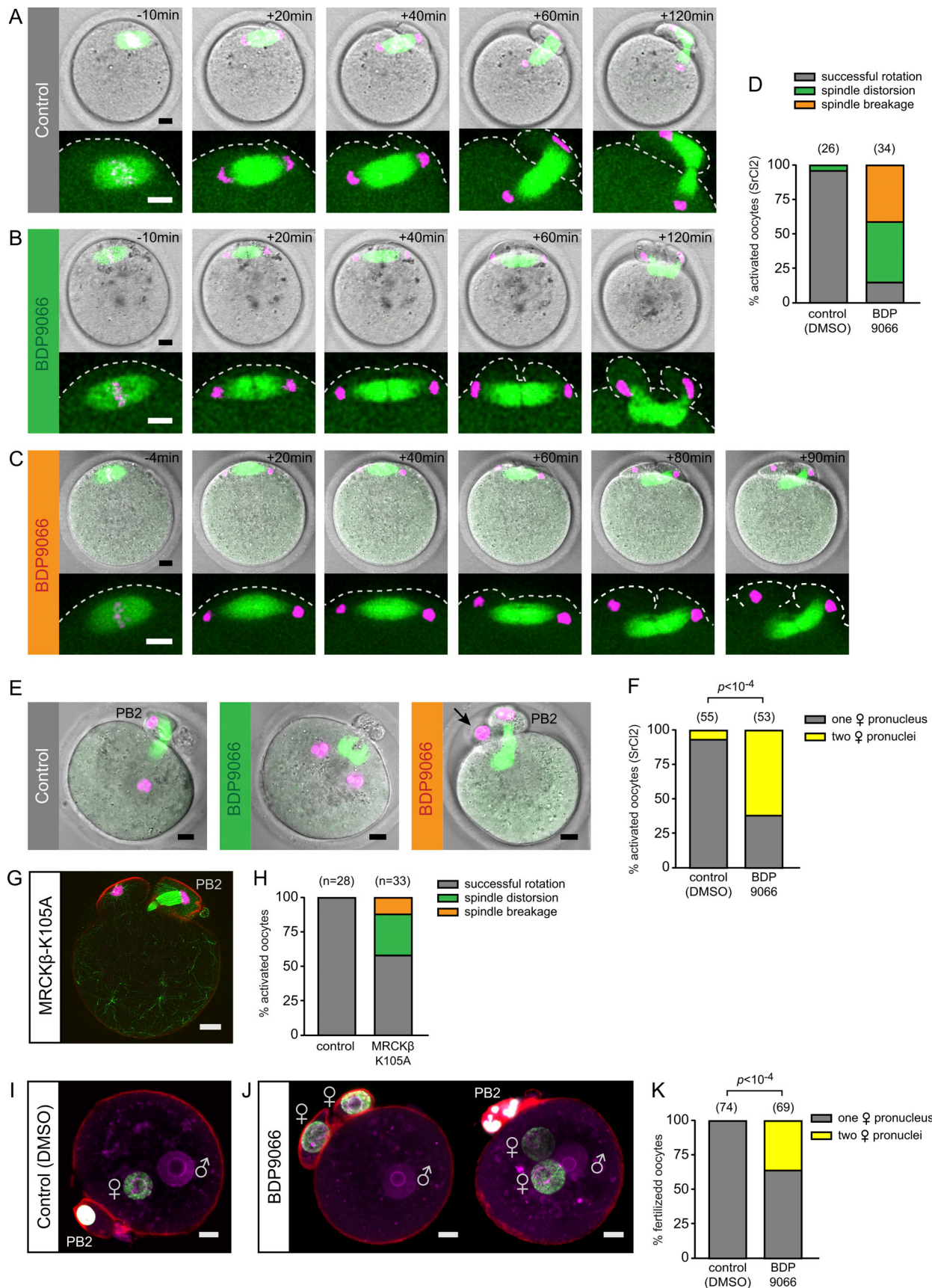


Figure 5. MRCK promotes spindle rotation in anaphase II. **(A)** Time-lapse images of anaphase II in a live SrCl_2 -activated MII oocyte, relative to the onset of chromatid segregation ($t = 0$). Before activation, MII oocytes were injected with cRNAs encoding EGFP-MAP4 to label microtubules and H2B-mCherry to label

chromosomes. The oocyte was treated with DMSO as a control. Images in the top row are compressed z-stacks of the microtubule and chromosome channels, spanning the entire spindle apparatus, combined with a single-plane brightfield image. The bottom row shows an expanded view of the spindle. Images are from [Video 2](#). **(B)** Time-lapse images of anaphase II in a live SrCl₂-activated MII oocyte treated with BDP9066. The experiment illustrates the spindle distortion phenotype. Images are from [Video 3](#). **(C)** Time-lapse images of anaphase II in a live SrCl₂-activated MII oocyte treated with BDP9066. The experiment illustrates the spindle breakage phenotype. Images are from [Video 4](#). **(D)** Bar graph depicting the fraction of activated oocytes (%), treated with DMSO or BDP9066, showing normal spindle rotation, the spindle distortion phenotype, or the spindle breakage phenotype. **(E)** Maternal PN configuration in SrCl₂-activated oocytes treated with DMSO (left) or BDP9066 (middle, right). Before activation, MII oocytes were injected with cRNAs encoding EGFP-MAP4 to label microtubules and H2B-mCherry to label chromosomes. Activated oocytes were imaged live 6 h after activation. In the middle image, the BDP9066-treated oocyte shows two maternal pronuclei and a distorted anaphase II spindle remnant, suggestive of spindle distortion during anaphase II. In the right image, the BDP9066-treated oocyte shows a second polar body and a maternal PN enclosed in a polar body-like protrusion (arrow), suggestive of spindle breakage during anaphase II. **(F)** Bar graph depicting the fraction (%) of activated oocytes containing a single maternal PN (gray), or two maternal pronuclei (yellow), when scored 6 h after activation. Oocytes were activated in the presence of DMSO or BDP9066 (1 μM) as shown in E. P value was calculated using Fisher's exact test. **(G)** Spindle breakage phenotype in an SrCl₂-activated MII oocyte expressing MRCKβ-K105A. The oocyte was fixed 1.5 h after activation, then stained for tubulin (green), chromatin (TO-PRO-3; magenta), and F-actin (Alexa Fluor 568-phalloidin; red). The image is a compressed z-stack of 18 consecutive confocal frames taken from [Video 5](#) spanning the entire spindle apparatus. For clarity, a single image of the F-actin channel was overlaid. **(H)** Bar graph depicting the fraction (%) of SrCl₂-activated oocytes injected with water (control) or with MRCKβ-K105A cRNA, showing normal spindle rotation, spindle distortion, or spindle breakage, when scored 1.5 h after activation. **(I)** Pronuclei staining in a control zygote, obtained by in vitro fertilization in the presence of DMSO. The zygote was fixed 6.5 h after insemination and stained for H3K4me3 (green), F-actin (Alexa Fluor 568-phalloidin; red), and chromatin (TO-PRO-3; magenta). **(J)** Pronuclei staining in zygotes obtained by in vitro fertilization in the presence of BDP9066. Zygotes were fixed and stained as in I. The left image illustrates the presence of two maternal pronuclei, each enclosed in a polar body-like protrusion. The right image illustrates the presence of two maternal pronuclei located deeper in the cytoplasm. **(K)** Bar graph depicting the fraction (%) of fertilized oocytes containing a single maternal PN (gray) or two maternal pronuclei (yellow) when fixed 6.5 h after insemination. Oocytes were fertilized in the presence of DMSO or BDP9066 (2 μM) as shown in I and J. P value was calculated using Fisher's exact test. The number of oocytes scored is indicated in parentheses above each bar. Scale bars are 10 μm.

congressed to the center of the cell ([Maro et al., 1984](#)). As expected, control zygotes exhibited closely apposed expanded male and female pronuclei located near the center of the zygote ([Fig. 6, E and F](#)). Notably, the male PN was located at a distance from the cortex, demonstrating successful migration away from the sperm entry site ([Fig. 6, E and F](#)). In striking contrast, male pronuclei demonstrated a complete failure of migration in MRCK-inhibited zygotes and remained apposed to an actin-rich remnant of the FC ([Fig. 6, E and F](#)). In the same fashion, oocytes expressing kinase-dead MRCKβ-K105A showed a strong impairment of male PN migration after fertilization ([Fig. 6, G–I](#)). However, these zygotes did not show significant bulging of the FC, presumably because ring myosin II inhibition occurred before sperm fusion. Together, these data suggest that the MRCK/myosin II pathway orchestrates both FC bulging and flattening to eventually produce inward-directed forces that will initiate male PN migration.

Discussion

Despite being a signature of mouse oocyte polarization, the mechanism and rationale for ring myosin II activation have been little investigated. The myosin II ring was first thought to reflect a preassembled—yet unproductive—actomyosin ring for PB2 cytokinesis ([Deng et al., 2007; Yi and Li, 2012](#)). However, we and others have shown that the driving force for unilateral membrane furrowing and PB2 formation is the RhoA-dependent activation of the ROCK/myosin II pathway above the central spindle ([Zhong et al., 2005; Dehapiot et al., 2021](#)). A major obstacle has been the lack of tools to inhibit ring myosin II specifically, without affecting ROCK/myosin II—as general myosin II inhibitors such as blebbistatin would do. Our data provide a solution to tackle this issue as we identify MRCK as the myosin light chain kinase acting downstream of Cdc42 to specifically activate ring myosin II, in both MII and anaphase II.

Our data challenge the prevailing view that ring myosin II activation is driven by MLCK, based on the use of compound ML-7. Though ML-7 has not been formally tested against MRCK, it seems plausible that high concentrations may impact MRCK activity. In this regard, apical constriction of endoderm precursor cells in *Caenorhabditis elegans* gastrulation was initially reported to rely on MLCK for myosin II activation, based on the use of ML-7, but was later found to actually rely on MRCK ([Lee and Goldstein, 2003; Marston et al., 2016](#)). In mouse oocytes, conflicting results have been reported as to whether ML-7 inhibits PB2 emission ([Matson et al., 2006; Larson et al., 2010; Ajduk et al., 2011; Wang et al., 2011; McGinnis et al., 2015](#)). Moreover, oocyte-specific invalidation of the *Mylk1* gene, which encodes smooth muscle and nonmuscle MLCK, suggested that MLCK is dispensable for oocyte maturation, fertilization, and polar body emission ([Liang et al., 2015](#)). These observations call for caution regarding previously reported roles for MLCK in mouse oocytes.

The loss of ring myosin II in MII oocytes did not produce a remarkable phenotype, aside from a flattening of the polarized cortex, thus highlighting a role for ring myosin II in producing cortical tension for membrane deformation. Yet, the extent of bulging is variable among oocytes and its biological significance remains elusive. Intriguingly, we also observed a shortening of the actin cap and a corresponding loss of Arp2/3 complex localization at the rim of the polarized cortex. From this observation, we infer that ring myosin II does not limit actin cap growth. Instead, formation of an actomyosin network may stabilize actin filaments in the transition zone between the actin cap and the microvillar cortex, thereby promoting the widening of the actin-rich cortex. Therefore, ring myosin II extends the effect of the Ran-GTP gradient in setting the size of the polarized Arp2/3 domain and the actin cap. Future studies may identify new roles for ring myosin II during MII arrest. For instance, the myosin II ring could perhaps contribute to establishing a

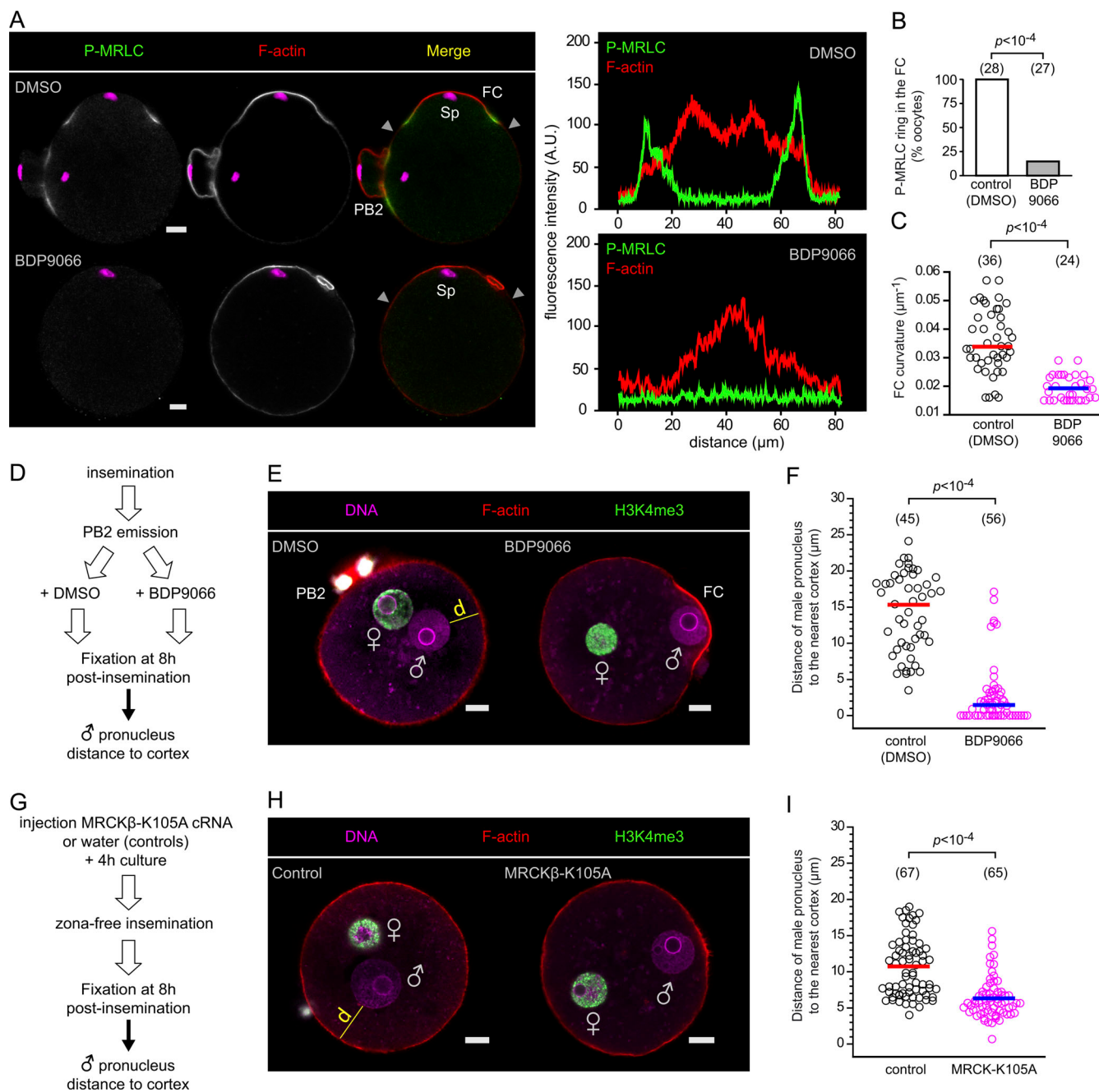


Figure 6. MRCK promotes myosin II activation in the FC and male PN centration. **(A)** Immunofluorescence detection of activated myosin II (P-MRLC) in fertilized oocytes. Top row: Control oocyte treated with DMSO. Bottom row: Oocyte fertilized in the presence of BDP9066 (2 μM). Note the P-MRLC ring at the base of the FC in the control oocyte and the absence in the MRCK-inhibited oocyte. Oocytes were fixed 3 h after insemination. Fluorescence intensity profiles correspond to the cortical regions delineated by the gray arrowheads in the merge images. **(B)** Bar graph depicting the fraction of fertilized oocytes showing a P-MRLC ring at the base of the FC, as shown in A. The fertilization medium was supplemented with DMSO (control) or BDP9066 (2 μM). **(C)** Scatter plot of the average curvature of the FC. **(D)** Schematic illustrating the experimental protocol for monitoring male PN migration after zona-intact fertilization. **(E)** Detection of male and female pronuclei in zygotes fixed 8 h after insemination. The left image shows a control zygote treated with DMSO after PB2 emission. The yellow line denotes the distance (d) of the male PN to the nearest cortex. The right image shows a zygote treated with BDP9066 (2 μM) after PB2 emission. Note the expanded male PN still apposed to the FC cortex. Images are z-compressions of two consecutive confocal frames. **(F)** Scatter plot of the male PN distance to the nearest cortex, as depicted in E. **(G)** Schematic illustrating the experimental protocol for monitoring male PN migration after injection and zona-free fertilization. **(H)** Detection of male and female pronuclei in zygotes fixed 8 h after zona-free insemination. The left image shows a control zygote injected with water. The yellow line denotes the distance (d) of the male PN to the nearest cortex. The right image shows a zygote expressing MRCK β -K105A. **(I)** Scatter plot of the male PN distance to the nearest cortex, as depicted in H. Red and blue horizontal bars indicate means (C and I) or medians (F). P values were calculated using Fisher's exact test (B), two-tailed Student's *t* test (C and I), or a two-tailed Mann-Whitney U test (F). The number of oocytes scored is indicated in parentheses above each bar/scatter plot. Scale bars are 10 μm . Chromosomes were stained with TO-PRO-3 (magenta). F-actin was labeled with Alexa Fluor 568-phalloidin. In E and H, female pronuclei were immuno-stained for H3K4me3 (green). Sp: sperm chromatin.

diffusion barrier for the segregation of proteins that belong to the polarized cortex from those which don't, such as sperm-binding proteins (Inoue et al., 2020; Mori et al., 2021).

Activated oocytes, in contrast, exhibited striking spindle rotation defects in the absence of ring myosin II. The dramatic spindle bending and breaking phenotypes are highly suggestive of a tug-of-war between furrow ingression, which exerts an inward pushing force on the anaphase II spindle (Dehapiot et al., 2021), and the chromatin clusters, which seem to mediate spindle pole anchoring to the cortex. Remarkably, this tug-of-war could ultimately lead to the anaphase spindle parting from one chromatid cluster, effectively rescuing rotation. Hence, these data reveal that spindle rotation and PB2 extrusion can be achieved in oocytes lacking ring myosin II, providing unambiguous evidence that the MRCK-driven myosin II ring is not the precursor of the cytokinetic ring. These findings substantiate our model of spindle rotation being driven primarily by ROCK-induced cortical ingression, providing the anaphase II spindle can break its symmetrical anchoring to the cortex (Dehapiot et al., 2021).

In view of the persistent cortical anchoring of the detached chromatid cluster, resisting the drag of the rotating spindle, we infer that the requirement for ring myosin II during spindle rotation may lie in preventing the chromatid clusters at spindle poles from sticking too tight to the cortex to facilitate symmetry breaking. It is notorious that chromosomes can firmly stick to the oocyte cortex when at close range, e.g., following MII spindle disassembly with microtubule poisons (Longo and Chen, 1985; Maro et al., 1984; Dehapiot et al., 2013; Yi et al., 2011). While the molecular underpinnings of this anchoring remain to be fully elucidated, evidence suggests that cytoplasmic streaming powered by actin flow may provide a net pushing force upon MII chromosomes (Yi et al., 2011). Accordingly, we have previously reported that acute exposure to a low dose of nocodazole during spindle rotation resulted in the internalized chromatid cluster detaching from the spindle pole to reach toward and stick to the nearby cortex (Dehapiot et al., 2021). The function of ring myosin II could be to provide tension for localized membrane bulging above the two sets of segregated chromatids during the early stages of anaphase II, so as to prevent the chromatid clusters from reaching too close to the cortex, which would result in irreversible anchoring. Further investigations are required to test this scenario.

The sporadic rescue of spindle rotation through chromatid disengagement indicates that oocytes may proceed with normal embryonic development in the absence of ring myosin II. Consistent with this idea, the conditional deletion of myosin IIA in oocytes resulted in subfertility, whereby female mice produced litters that were half the size of control litters (Vogt et al., 2019). While the molecular underpinnings of this subfertility were not elucidated, our work suggests that it may have arisen from defective PB2 extrusion in a subset of oocytes. Accordingly, two-cell embryos derived from oocytes lacking maternal myosin IIA were found to contain an extra nucleus in one blastomere (Vogt et al., 2019, Fig. 6). Moreover, the same study reported that conditional deletion of the oocyte-specific protein Mater, a component of the subcortical maternal complex, resulted in a

dramatic decrease of myosin IIA expression in MII oocytes, associated with an increased incidence of tripromuclear zygotes (Vogt et al., 2019). While the study did not demonstrate the origin of the extra PN, we surmise, in light of our data, that the extra PN may originate from PB2 extrusion failure. Together with our findings, these data warrant further investigations into the role of the MRCK/myosin IIA pathway in the formation of digynic tripromuclear zygotes, a frequently observed abnormal outcome of in vitro fertilization in the clinic (Ezoe et al., 2022).

Much similar to the polarized cortex overlying maternal chromosomes, we uncovered that the FC involves the Cdc42/MRCK pathway for ring myosin II activation, consistent with chromatin—whether maternal or paternal—acting as the upstream polarization cue (Deng et al., 2007; Deng and Li, 2009). The male PN forms within the FC and must therefore be actively translocated toward the center of the zygote for apposition with the female PN ahead of the first embryonic mitosis. It was recently demonstrated that male PN migration occurs in two phases: first, a fast migratory phase relying on actin filaments promotes male PN launching away from the cortex; next, a slow centration phase relying on microtubule dynamics finalizes pronuclei apposition (Scheffler et al., 2021). Intriguingly, the initial male PN launching coincides with the flattening of the FC, the mechanism of which had remained elusive. Accordingly, it was suggested that FC flattening initiates male PN migration; however, this was not demonstrated experimentally (Scheffler et al., 2021). Here, we show that ring myosin II plays a dual role in FC dynamics: first, it is required for FC outward protrusion, similar to its role in cortical bulging above the MII spindle; next, FC myosin II is required to flatten the FC after male PN formation, effectively providing a molecular basis for the earliest and decisive step of male PN migration. One may then speculate on the requirement for myosin II for PN launching. By analogy with the signaling cascade elicited by maternal chromosomes, activation of the Cdc42/MRCK pathway in the FC may rely on a Ran-GTP signal generated by sperm chromatin. Pronuclear membrane formation, which occurs concurrently with FC flattening (Scheffler et al., 2021), would thus be expected to shut down this polarizing cue. Hence, FC flattening may result from the transient reorganization of FC myosin II into a contractile cortical cap, similar to what was reported in MII oocytes in which Ran GTPase was inactivated (Deng et al., 2007), and in the flattening protrusion overlying the internalized chromatid cluster during spindle rotation (Wang et al., 2020; Dehapiot et al., 2021). Further investigations are required to substantiate this model and explore in more detail the dynamics of myosin II in the flattening cone.

MRCK has recently emerged as a new player in actomyosin contractility in a variety of mammalian systems, including epithelial homeostasis, cell adhesion, and phagocytosis (Ando et al., 2013; Marston et al., 2016; Gagliardi et al., 2018; Zihni et al., 2017, 2022; Zihni, 2021). MRCK was also implicated in the regulation of cell motility and invasiveness and could provide a druggable target in several cancers (Tan et al., 2008; Unbekandt and Olson, 2014; Unbekandt et al., 2018; Kurimchak et al., 2020; East and Asquith, 2021). Here, we have shown that MRCK is also an important Cdc42 effector in promoting cortical myosin II activation

for mouse oocyte polarization and asymmetric division. Since this signaling cascade occurs when maternal/paternal chromatin is in close vicinity to the cortex, it is reasonable to speculate that it may be conserved in oocytes from other species. Intriguingly, a recent study by Pelzer and colleagues reported that the pathway for chromosome-induced cortical contractility remains active in preimplantation embryos and may lead to blastomere fragmentation if mitotic chromosomes come near the cortex for an extended duration (Pelzer et al., 2023). In dividing somatic cells however, the scenario is quite the opposite, as Ran-GTP was shown to promote myosin II depletion from the chromosome-proximal polar cortex, thereby allowing for membrane expansion (Kiyomitsu and Cheeseman, 2013). Yet, myosin II organization as a ring seems to be particularly suited to producing a membrane bulge with a defined boundary. In line with this idea, myosin II rings orchestrate the bending of cortical F-actin caps, and the buckling of the cell cortex during furrowing of the syncytial *Drosophila* embryo (Zhang et al., 2018).

It is likely that yet new roles for MRCK will emerge in future studies, including perhaps within the context of oocyte maturation or preimplantation embryo development. While this study focused on MRCK β , which was readily detectable in the polarized cortex, transcripts encoding both MRCK β and the closely related MRCK α are found in mouse MII oocytes and are likely actively translated (Hu et al., 2022). Yet, mice lacking MRCK α are viable and fertile, arguing against an essential role for this isoform during normal development (Kwa et al., 2021). Further studies involving invalidation strategies at the gene or protein level will be required to clarify the respective contribution of each isoform, or whether they act redundantly, in driving ring myosin II activation. Other pools of activated myosin II are likely to be encountered away from the polarized cortex, such as in association with the dynamic actin network that fills the oocyte cytoplasm or, as described recently, in association with cortical granules (Vogt et al., 2019). Whether these alternative myosin II pools rely on the activation of the Cdc42/MRCK pathway at the polarized cortex or in more discrete cytoplasmic compartments remains an open question.

Materials and methods

Mice

All animal procedures were conducted in accordance with the European directive for the use and care of laboratory animals (2010/63/EU) and approved by the local animal ethics committee under the French Ministry of Higher Education, Research and Innovation (Project license APAFIS#11761-2017101200282520). Mice of the MF1 strain were initially purchased from Envigo and maintained as a colony in the local animal facility.

Oocyte recovery and culture

To minimize the number of animals, female mice (6–8 wk old) were primed by intraperitoneal injection of 5–7 U of pregnant mare serum gonadotropin (Chronogest, MSD), followed 48 h later by 5 IU human chorionic gonadotropin (Chorulon, MSD). MII oocytes were recovered from the oviducts in M2 medium (Sigma-Aldrich) supplemented with 3 mg/ml hyaluronidase

(Sigma-Aldrich), followed by wash. Oocytes were subsequently cultured in homemade M16 medium (Nagy et al., 2003) in an incubator providing an atmosphere of 5% CO₂ in air. To achieve Ca²⁺ depletion, MII oocytes were cultured for 1 h in Ca²⁺-free M16 medium supplemented with 1 mM EGTA and containing 10 μM thapsigargin (Tocris) to promote intracellular Ca²⁺ store depletion (Swann, 1994; Kline and Kline, 1992a; Miao et al., 2012). To induce artificial resumption of meiosis II, MII oocytes were cultured in Ca²⁺-free M16 medium supplemented with 10 mM SrCl₂ (Kline and Kline, 1992b).

Inhibitor treatments

The following small molecule inhibitors were used: ML-141 (5 μM; Tocris), ML-7 (15 μM; Tocris), Wortmannin (1 μM; Echelon biosciences), IPA-3 (1 μM; Tocris), BDP9066 (1 μM; Aobious), CK-666 (100 μM; Sigma-Aldrich), and Y-27632 (50 μM; Merck Millipore). An equivalent amount of DMSO was used for controls. Peptide-18 (Merck Millipore) was recovered in water at a stock concentration of 1 mg/ml and microinjected in the oocyte cytoplasm. In our preliminary experiments, we consistently noticed that oocytes cultured in media containing BSA required higher concentrations of inhibitors to obtain a full inhibition of the P-MRLC ring when compared with oocytes cultured in media in which BSA was substituted for poly(vinyl alcohol) (Sigma-Aldrich). Therefore, experiments involving inhibitor treatments were performed in homemade BSA-free M16 medium supplemented with 0.05% poly(vinyl alcohol). However, fertilization experiments involving BDP9066 were performed using commercial HTF medium, which contains 4 mg/ml BSA (Merck Technical Services, personal communication).

In vitro fertilization

Fertilization of MII oocytes was performed according to previously published protocols (Maro et al., 1984; Miao et al., 2012). Briefly, sperm recovered from 12–15-wk-old male MF1 mice was capacitated for 2 h in a 500-μl drop of equilibrated HTF medium (MR-070-D, MERCK Sigma-Aldrich) layered with mineral oil (Sigma-Aldrich) at 37°C in a 5% CO₂ incubator. Cumulus masses were recovered from the oviducts 13 h after human chorionic gonadotropin and were placed in a culture dish containing 2.4 ml of equilibrated HTF to which 50 μl of the capacitated sperm suspension was added. The dish was returned to the incubator for fertilization to proceed. After 3 h, oocytes were transferred to a new dish of equilibrated HTF medium to wash out unbound sperm. Fertilized oocytes were recovered at various times after insemination for further analysis. To facilitate the fertilization of oocytes that had been microinjected with the cRNA encoding the Cdc42-GTP biosensor or the kinase-dead MRCK β -K105A, the zona pellucida was removed by a brief incubation in acidic Tyrode's solution (Sigma-Aldrich) at 37°C.

Immunofluorescence and staining

Oocytes were fixed for 30 min at room temperature with paraformaldehyde 3% in PBS, freshly prepared from a 16% methanol-free paraformaldehyde solution (Electron Microscopy Sciences). Fixed oocytes were permeabilized with 0.1% Triton X-100 (Sigma-Aldrich) in PBS for 15 min at room temperature.

After blocking with 3% BSA (Sigma-Aldrich) in PBS for 2 h, oocytes were incubated overnight at 4°C with primary antibodies in PBS-BSA 3%. The next day, oocytes were washed in PBS-BSA 3% and incubated with secondary antibodies diluted 1:1,000 in PBS-BSA 1% for 45 min at 37°C. The following primary antibodies were used: phospho-myosin light chain 2 (Ser19; 1:200; #3671; Cell Signaling Technology), non-muscle myosin IIA (1:100; ab24762; Abcam), myosin IIB (D8H8; 1:100; #8824; Cell Signaling Technology), MRCK β (A-2; 1:100; sc-390127; Santa Cruz Biotechnology), tubulin (1:200; ab6161; Abcam), p34-ARC (1:100; sc-515754; Santa Cruz Biotechnology), Rock-1 (K-18; 1:100; sc-6056; Santa Cruz Biotechnology), and trimethyl-histone H3 Lys4 (1:100; 04-745; Merck Millipore). Secondary antibodies were Alexa Fluor 488-conjugated donkey anti-goat, donkey anti-rabbit and goat anti-rat, and Alexa Fluor 555-conjugated goat anti-mouse and goat anti-rabbit (all 1:1,000; Invitrogen). Actin filaments were stained with Alexa Fluor 568-phalloidin (Life Technologies). Chromatin was stained with TO-PRO-3 (Invitrogen) or SiRNA (Spirochrome).

Plasmids, cRNA preparation, and microinjection

The following plasmids were used: H2B-mCherry in pcDNA3 (Robert Benzera; plasmid #20972; Addgene) and pGEMHE-eGFP-MAP4 (Jan Ellenberg; plasmid #P30518; Euroscarf). MRCK β -EGFP and MRCK β (H1593/1596A)-EGFP in pEGFP-N1 were kindly donated by Prof. Shigetomo Fukuhara (Institute of Advanced Medical Science, Tokyo, Japan) and were subcloned into pcDNA3.1. The pEGFP-RhoA Biosensor was from Michael Glotzer (plasmid #68026; Addgene) and was subcloned into pcDNA3.1 while replacing EGFP with mCherry. Polyadenylated cRNAs were synthesized in vitro from linearized plasmids using the mMessage mMachine T7 kit and Poly(A) Tailing kit (Ambion), then purified with RNeasy purification kit (Qiagen), and stored at -80°C. MII oocytes were injected with ~5 pl cRNA solution and cultured for at least 2 h to allow for protein expression.

Confocal imaging and image processing

For immunofluorescence experiments, oocytes were placed on glass-bottom dishes (MatTek) in a small drop of PBS-BSA 1% supplemented with TO-PRO-3 and covered with mineral oil. Fixed oocytes were imaged with a Leica SP5 or SP8 confocal microscope using a 63 \times oil-immersion objective. When appropriate, displayed confocal images were cropped so as to hide excessive non-specific signals arising from the zona pellucida. For live imaging of meiosis resumption and PB2 formation, oocytes were deposited at the center of a glass-bottom dish (MatTek) filled with 2 ml of Ca²⁺-free and BSA-free M16 medium containing 10 mM SrCl₂. Time-lapse recordings were acquired with a Leica SP8 confocal microscope using 20 \times or 40 \times oil-immersion objectives. The temperature was maintained at 37°C using a stage top incubator (INUBG2E-GSI; Tokai Hit) fitted on the microscope stage. Confocal image thickness was set to 1 μ m. Confocal images and time-lapse movies were processed with Fiji. Fluorescence intensity profiles were obtained using the segmented line tool (width 10 pixels) and the Plot Profile function in Fiji. For quantification of P-MRLC staining in Fig. S2,

fluorescence intensity profiles were obtained using the segmented line tool (width 20 pixels), adjusted for background subtraction, and the area under the curve was taken as a readout of P-MRLC staining intensity. Measurements of the chromosome distance to the cortex and male PN distance to the cortex were realized using the Leica LAS AF Lite 2.6.0 software. The extent of FC protrusion was quantified using the Fiji plugin Kappa for curvature analysis (Mary and Brouhard, 2019 Preprint) in zygotes fixed 3 h after insemination. Briefly, a curve (length 130 μ m; thickness 1 pixel) was manually drawn along the cortical F-actin layer overlying sperm chromatin and an average curvature value (in μ m⁻¹) was obtained after B-spline curve fitting and used as a proxy for outward protrusion.

Statistical analysis

Statistical analyses were performed using Fisher's exact test, two-tailed Student's *t* test, or two-tailed Mann-Whitney U test, in Origin (OriginLab) or GraphPad QuickCalcs (<http://graphpad.com>). Statistical significance was considered when *P* < 0.05. Graphics (fluorescence intensity profiles, box plots, and scatter plots) were produced in Origin. Box plots show the median (line), 25th and 75th percentile (box), and fifth and 95th percentile (whiskers).

Online supplemental material

Fig. S1 shows the immuno-detection of myosin IIA and myosin IIB heavy chains in MII and anaphase II oocytes. **Fig. S2** shows the unaltered activation of ring myosin II in MII oocytes treated with inhibitors targeting MLCK or group I PAKs. **Fig. S3** shows the design of the Cdc42-GTP biosensor. **Fig. S4** shows that the Cdc42/MRCK β /myosin II pathway is activated in the FC. **Video 1** shows the flattening of the bulge in an MII oocyte treated with BDP9066. **Video 2** shows spindle rotation and PB2 emission in a control oocyte activated with SrCl₂. **Video 3** shows spindle distortion in an SrCl₂-activated oocyte treated with BDP9066. **Video 4** shows the rescue of spindle rotation and PB2 emission by means of spindle breakage in an SrCl₂-activated oocyte treated with BDP9066. **Video 5** shows a confocal z-stack across an SrCl₂-activated oocyte expressing MRCK β -K105A and showing the spindle breakage phenotype.

Data availability

The data reported in this article are available in the published article and its online supplemental material.

Acknowledgments

We thank Prof. Shigetomo Fukuhara (Institute of Advanced Medical Science, Tokyo, Japan) for kindly providing the plasmids encoding MRCK β -EGFP and MRCK β (H1593/1596A)-EGFP. We are grateful to the staff of the Animalerie Rennaise Centre d'Hébergement et d'Expérimentation-Biosit animal facility and Microscopy Rennes Imaging Center-Biosit microscopy facility for technical assistance and expert advice.

This work was supported by institutional funds from Centre National de la Recherche Scientifique. B. Dehapiot received a PhD scholarship from the French Ministry of Research and

Higher Education and additional funding from the Fondation pour la Recherche Médicale.

Author contributions: Conceptualization: A. Bourdais, B. Dehapiot, and G. Halet; Formal analysis: A. Bourdais, B. Dehapiot, and G. Halet; Funding acquisition: G. Halet; Investigation: A. Bourdais, B. Dehapiot, and G. Halet; Methodology: A. Bourdais, B. Dehapiot, and G. Halet; Project administration: G. Halet; Resources: A. Bourdais, B. Dehapiot, and G. Halet; Supervision: G. Halet; Validation: A. Bourdais, B. Dehapiot, and G. Halet; Visualization: A. Bourdais, B. Dehapiot, and G. Halet; Writing—original draft: A. Bourdais, B. Dehapiot, and G. Halet; Writing—review and editing: A. Bourdais, B. Dehapiot, and G. Halet.

Disclosures: The authors declare no competing interests exist.

Submitted: 8 November 2022

Revised: 24 June 2023

Accepted: 9 August 2023

References

- Ajduk, A., T. Ilozue, S. Windsor, Y. Yu, K.B. Seres, R.J. Bomphrey, B.D. Tom, K. Swann, A. Thomas, C. Graham, and M. Zernicka-Goetz. 2011. Rhythmic actomyosin-driven contractions induced by sperm entry predict mammalian embryo viability. *Nat. Commun.* 2:417. <https://doi.org/10.1038/ncomms1424>
- Amano, M., M. Ito, K. Kimura, Y. Fukata, K. Chihara, T. Nakano, Y. Matsuura, and K. Kaibuchi. 1996. Phosphorylation and activation of myosin by Rho-associated kinase (Rho-kinase). *J. Biol. Chem.* 271:20246–20249. <https://doi.org/10.1074/jbc.271.34.20246>
- Ando, K., S. Fukuwara, T. Moriya, Y. Obara, N. Nakahata, and N. Mochizuki. 2013. Rap1 potentiates endothelial cell junctions by spatially controlling myosin II activity and actin organization. *J. Cell Biol.* 202:901–916. <https://doi.org/10.1083/jcb.201301115>
- Beach, J.R., K.S. Bruun, L. Shao, D. Li, Z. Swider, K. Remmert, Y. Zhang, M.A. Conti, R.S. Adelstein, N.M. Rusan, et al. 2017. Actin dynamics and competition for myosin monomer govern the sequential amplification of myosin filaments. *Nat. Cell Biol.* 19:85–93. <https://doi.org/10.1038/ncb3463>
- Bourdais, A., B. Dehapiot, and G. Halet. 2021. Cofilin regulates actin network homeostasis and microvilli length in mouse oocytes. *J. Cell Sci.* 134: jcs259237. <https://doi.org/10.1242/jcs.259237>
- Chaigne, A., M.H. Verlhac, and M.E. Terret. 2012. Spindle positioning in mammalian oocytes. *Exp. Cell Res.* 318:1442–1447. <https://doi.org/10.1016/j.yexcr.2012.02.019>
- Chew, T.L., R.A. Masaracchia, Z.M. Goeckeler, and R.B. Wysolmerski. 1998. Phosphorylation of non-muscle myosin II regulatory light chain by p21-activated kinase (γ -PAK). *J. Muscle Res. Cell Motil.* 19:839–854. <https://doi.org/10.1023/A:1005417926585>
- Clift, D., and M. Schuh. 2013. Restarting life: Fertilization and the transition from meiosis to mitosis. *Nat. Rev. Mol. Cell Biol.* 14:549–562. <https://doi.org/10.1038/nrm3643>
- Coué, M., S.L. Brenner, I. Spector, and E.D. Korn. 1987. Inhibition of actin polymerization by latrunculin A. *FEBS Lett.* 213:316–318. [https://doi.org/10.1016/0014-5793\(87\)81513-2](https://doi.org/10.1016/0014-5793(87)81513-2)
- Davies, S.P., H. Reddy, M. Caivano, and P. Cohen. 2000. Specificity and mechanism of action of some commonly used protein kinase inhibitors. *Biochem. J.* 351:95–105. <https://doi.org/10.1042/bj3510095>
- Deacon, S.W., A. Beeser, J.A. Fukui, U.E.E. Rennefahrt, C. Myers, J. Chernoff, and J.R. Peterson. 2008. An isoform-selective, small-molecule inhibitor targets the autoregulatory mechanism of p21-activated kinase. *Chem. Biol.* 15:322–331. <https://doi.org/10.1016/j.chembiol.2008.03.005>
- Dehapiot, B., V. Carrière, J. Carroll, and G. Halet. 2013. Polarized Cdc42 activation promotes polar body protrusion and asymmetric division in mouse oocytes. *Dev. Biol.* 377:202–212. <https://doi.org/10.1016/j.ydbio.2013.01.029>
- Dehapiot, B., and G. Halet. 2013. Ran GTPase promotes oocyte polarization by regulating ERM (Ezrin/Radixin/Moesin) inactivation. *Cell Cycle.* 12: 1672–1678. <https://doi.org/10.4161/cc.24901>
- Dehapiot, B., R. Clément, A. Bourdais, V. Carrière, S. Huet, and G. Halet. 2021. RhoA- and Cdc42-induced antagonistic forces underlie symmetry breaking and spindle rotation in mouse oocytes. *PLoS Biol.* 19:e3001376. <https://doi.org/10.1371/journal.pbio.3001376>
- Deng, M., C.J. Williams, and R.M. Schultz. 2005. Role of MAP kinase and myosin light chain kinase in chromosome-induced development of mouse egg polarity. *Dev. Biol.* 278:358–366. <https://doi.org/10.1016/j.ydbio.2004.11.013>
- Deng, M., P. Suraneni, R.M. Schultz, and R. Li. 2007. The Ran GTPase mediates chromatin signaling to control cortical polarity during polar body extrusion in mouse oocytes. *Dev. Cell.* 12:301–308. <https://doi.org/10.1016/j.devcel.2006.11.008>
- Deng, M., and R. Li. 2009. Sperm chromatin-induced ectopic polar body extrusion in mouse eggs after ICSI and delayed egg activation. *PLoS One.* 4:e7171. <https://doi.org/10.1371/journal.pone.0007171>
- East, M.P., and C.R.M. Asquith. 2021. CDC42BPA/MRCKα: A kinase target for brain, ovarian and skin cancers. *Nat. Rev. Drug Discov.* 20:167. <https://doi.org/10.1038/d41573-021-00023-9>
- Ezoe, K., T. Takahashi, K. Shimazaki, T. Miki, Y. Tanimura, A. Amagai, A. Sawado, H. Akaike, M. Mogi, S. Kaneko, et al. 2022. Human 1PN and 3PN zygotes recapitulate all morphokinetic events of normal fertilization but reveal novel developmental errors. *Hum. Reprod.* 37:2307–2319. <https://doi.org/10.1093/humrep/deac177>
- Gagliardi, P.A., D. Somale, A. Puliafito, G. Chiaverina, L. di Blasio, M. Oneto, P. Bianchini, F. Bussolino, and L. Primo. 2018. MRCKα is activated by caspase cleavage to assemble an apical actin ring for epithelial cell extrusion. *J. Cell Biol.* 217:231–249. <https://doi.org/10.1083/jcb.201703044>
- Heissler, S.M., and J.R. Sellers. 2016. Various themes of myosin regulation. *J. Mol. Biol.* 428:1927–1946. <https://doi.org/10.1016/j.jmb.2016.01.022>
- Hetrick, B., M.S. Han, L.A. Helgeson, and B.J. Nolen. 2013. Small molecules CK-666 and CK-869 inhibit actin-related protein 2/3 complex by blocking an activating conformational change. *Chem. Biol.* 20:701–712. <https://doi.org/10.1016/j.chembiol.2013.03.019>
- Hong, F., B.D. Haldeman, D. Jackson, M. Carter, J.E. Baker, and C.R. Cremo. 2011. Biochemistry of smooth muscle myosin light chain kinase. *Arch. Biochem. Biophys.* 510:135–146. <https://doi.org/10.1016/j.abb.2011.04.018>
- Hong, L., S.R. Kenney, G.K. Phillips, D. Simpson, C.E. Schroeder, J. Nöth, E. Romero, S. Swanson, A. Waller, J.J. Strouse, et al. 2013. Characterization of a Cdc42 protein inhibitor and its use as a molecular probe. *J. Biol. Chem.* 288:8531–8543. <https://doi.org/10.1074/jbc.M112.435941>
- Hu, W., H. Zeng, Y. Shi, C. Zhou, J. Huang, L. Jia, S. Xu, X. Feng, Y. Zeng, T. Xiong, et al. 2022. Single-cell transcriptome and translatome dualomics reveals potential mechanisms of human oocyte maturation. *Nat. Commun.* 13:5114. <https://doi.org/10.1038/s41467-022-32791-2>
- Inoue, N., T. Saito, and I. Wada. 2020. Unveiling a novel function of CD9 in surface compartmentalization of oocytes. *Development.* 147:dev189985. <https://doi.org/10.1242/dev.189985>
- Ishihara, H., B.L. Martin, D.L. Brautigan, H. Karaki, H. Ozaki, Y. Kato, N. Fusetani, S. Watabe, K. Hashimoto, D. Uemura, and D.J. Hartshorne. 1989. Calyculin A and okadaic acid: Inhibitors of protein phosphatase activity. *Biochem. Biophys. Res. Commun.* 159:871–877. [https://doi.org/10.1016/0006-291X\(89\)92189-X](https://doi.org/10.1016/0006-291X(89)92189-X)
- Kiyomitsu, T., and I.M. Cheeseman. 2013. Cortical dynein and asymmetric membrane elongation coordinately position the spindle in anaphase. *Cell.* 154:391–402. <https://doi.org/10.1016/j.cell.2013.06.010>
- Kline, D., and J.T. Kline. 1992a. Thapsigargin activates a calcium influx pathway in the unfertilized mouse egg and suppresses repetitive calcium transients in the fertilized egg. *J. Biol. Chem.* 267:17624–17630. [https://doi.org/10.1016/S0021-9258\(19\)37088-7](https://doi.org/10.1016/S0021-9258(19)37088-7)
- Kline, D., and J.T. Kline. 1992b. Repetitive calcium transients and the role of calcium in exocytosis and cell cycle activation in the mouse egg. *Dev. Biol.* 149:80–89. [https://doi.org/10.1016/0012-1606\(92\)90265-I](https://doi.org/10.1016/0012-1606(92)90265-I)
- Kuo, J.C., X. Han, C.T. Hsiao, J.R. Yates III, and C.M. Waterman. 2011. Analysis of the myosin-II-responsive focal adhesion proteome reveals a role for β -Pix in negative regulation of focal adhesion maturation. *Nat. Cell Biol.* 13:383–393. <https://doi.org/10.1038/ncb2216>
- Kurimchak, A.M., C. Herrera-Montávez, J. Brown, K.J. Johnson, V. Sodi, N. Srivastava, V. Kumar, S. Deihimi, S. O'Brien, S. Peri, et al. 2020. Functional proteomics interrogation of the kinome identifies MRCKα as a therapeutic target in high-grade serous ovarian carcinoma. *Sci. Signal.* 13:eaax8238. <https://doi.org/10.1126/scisignal.aax8238>
- Kwa, M.Q., R. Brandao, T.H. Phung, J. Ge, G. Scieri, and C. Brakebusch. 2021. MRCKα is dispensable for breast cancer development in the MMTV-PyMT model. *Cells.* 10:942. <https://doi.org/10.3390/cells10040942>

- Larson, S.M., H.J. Lee, P.H. Hung, L.M. Matthews, D.N. Robinson, and J.P. Evans. 2010. Cortical mechanics and meiosis II completion in mammalian oocytes are mediated by myosin-II and Ezrin-Radixin-Moesin (ERM) proteins. *Mol. Biol. Cell.* 21:3182–3192. <https://doi.org/10.1091/mbc.e10-01-0066>
- Lee, J.Y., and B. Goldstein. 2003. Mechanisms of cell positioning during *C. elegans* gastrulation. *Development*. 130:307–320. <https://doi.org/10.1242/dev.00211>
- Lepikhov, K., and J. Walter. 2004. Differential dynamics of histone H3 methylation at positions K4 and K9 in the mouse zygote. *BMC Dev. Biol.* 4:12. <https://doi.org/10.1186/1471-213X-4-12>
- Leung, T., X.Q. Chen, I. Tan, E. Manser, and L. Lim. 1998. Myotonic dystrophy kinase-related Cdc42-binding kinase acts as a Cdc42 effector in promoting cytoskeletal reorganization. *Mol. Cell. Biol.* 18:130–140. <https://doi.org/10.1128/MCB.18.1.130>
- Liang, Q.X., Q.H. Zhang, S.T. Qi, Z.W. Wang, M.W. Hu, X.S. Ma, M.S. Zhu, H. Schatten, Z.B. Wang, and Q.Y. Sun. 2015. Deletion of Mylk1 in oocytes causes delayed morula-to-blastocyst transition and reduced fertility without affecting folliculogenesis and oocyte maturation in mice. *Biol. Reprod.* 92:97. <https://doi.org/10.1095/biolreprod.114.122127>
- Lomakin, A.J., K.C. Lee, S.J. Han, D.A. Bui, M. Davidson, A. Mogilner, and G. Danuser. 2015. Competition for actin between two distinct F-actin networks defines a bistable switch for cell polarization. *Nat. Cell Biol.* 17:1435–1445. <https://doi.org/10.1038/ncb3246>
- Longo, F.J., and D.Y. Chen. 1985. Development of cortical polarity in mouse eggs: Involvement of the meiotic apparatus. *Dev. Biol.* 107:382–394. [https://doi.org/10.1016/0012-1606\(85\)90320-3](https://doi.org/10.1016/0012-1606(85)90320-3)
- Lukas, T.J., S. Mirzoeva, U. Slomczynska, and D.M. Watterson. 1999. Identification of novel classes of protein kinase inhibitors using combinatorial peptide chemistry based on functional genomics knowledge. *J. Med. Chem.* 42:910–919. <https://doi.org/10.1021/jm980573a>
- Mackenzie, A.C.L., D.D. Kyle, L.A. McGinnis, H.J. Lee, N. Aldana, D.N. Robinson, and J.P. Evans. 2016. Cortical mechanics and myosin-II abnormalities associated with post-ovulatory aging: Implications for functional defects in aged eggs. *Mol. Hum. Reprod.* 22:397–409. <https://doi.org/10.1093/molehr/gaw019>
- Maro, B., M.H. Johnson, S.J. Pickering, and G. Flach. 1984. Changes in actin distribution during fertilization of the mouse egg. *J. Embryol. Exp. Morphol.* 81:211–237. <https://doi.org/10.1242/dev.81.1.211>
- Marston, D.J., C.D. Higgins, K.A. Peters, T.D. Cupp, D.J. Dickinson, A.M. Pani, R.P. Moore, A.H. Cox, D.P. Kiehart, and B. Goldstein. 2016. MRCK-1 drives apical constriction in *C. elegans* by linking developmental patterning to force generation. *Curr. Biol.* 26:2079–2089. <https://doi.org/10.1016/j.cub.2016.06.010>
- Mary, H., and G.J. Brouhard. 2019. Kappa (κ): Analysis of curvature in biological image data using B-splines. *bioRxiv*. (Preprint posted November 25, 2019). <https://doi.org/10.1101/852772>
- Matson, S., S. Markoulaki, and T. Ducibella. 2006. Antagonists of myosin light chain kinase and of myosin II inhibit specific events of egg activation in fertilized mouse eggs. *Biol. Reprod.* 74:169–176. <https://doi.org/10.1095/biolreprod.105.046409>
- McGinnis, L.A., H.J. Lee, D.N. Robinson, and J.P. Evans. 2015. MAPK3/1 (ERK1/2) and myosin light chain kinase in mammalian eggs affect myosin-II function and regulate the metaphase II state in a calcium- and zinc-dependent manner. *Biol. Reprod.* 92:146. <https://doi.org/10.1095/biolreprod.114.127027>
- Miao, Y.L., P. Stein, W.N. Jefferson, E. Padilla-Banks, and C.J. Williams. 2012. Calcium influx-mediated signaling is required for complete mouse egg activation. *Proc. Natl. Acad. Sci. USA*. 109:4169–4174. <https://doi.org/10.1073/pnas.1112333109>
- Mogessie, B., K. Scheffler, and M. Schuh. 2018. Assembly and positioning of the oocyte meiotic spindle. *Annu. Rev. Cell Dev. Biol.* 34:381–403. <https://doi.org/10.1146/annurev-cellbio-100616-060553>
- Mori, M., T. Yao, T. Mishina, H. Endoh, M. Tanaka, N. Yonezawa, Y. Shimamoto, S. Yonemura, K. Yamagata, T.S. Kitajima, and M. Ikawa. 2021. RanGTP and the actin cytoskeleton keep paternal and maternal chromosomes apart during fertilization. *J. Cell Biol.* 220:e202012001. <https://doi.org/10.1083/jcb.202012001>
- Munjal, A., J.M. Philippe, E. Munro, and T. Lecuit. 2015. A self-organized biomechanical network drives shape changes during tissue morphogenesis. *Nature*. 524:351–355. <https://doi.org/10.1038/nature14603>
- Nagy, A., M. Gertsenstein, K. Vintersten, and R. Behringer. 2003. Manipulating the Mouse Embryo: A Laboratory manual. Third edition. Cold Spring Harbor Laboratory Press, Cold Spring Harbor, NY.
- Nakamura, N., N. Oshiro, Y. Fukata, M. Amano, M. Fukata, S. Kuroda, Y. Matsuura, T. Leung, L. Lim, and K. Kaibuchi. 2000. Phosphorylation of ERM proteins at filopodia induced by Cdc42. *Genes Cells*. 5:571–581. <https://doi.org/10.1046/j.1365-2443.2000.00348.x>
- Nakanishi, S., S. Kakita, I. Takahashi, K. Kawahara, E. Tsukuda, T. Sano, K. Yamada, M. Yoshida, H. Kase, and Y. Matsuda. 1992. Wortmannin, a microbial product inhibitor of myosin light chain kinase. *J. Biol. Chem.* 267:2157–2163. [https://doi.org/10.1016/S0021-9258\(18\)45857-7](https://doi.org/10.1016/S0021-9258(18)45857-7)
- Nolen, B.J., N. Tomasevic, A. Russell, D.W. Pierce, Z. Jia, C.D. McCormick, J. Hartman, R. Sakowicz, and T.D. Pollard. 2009. Characterization of two classes of small molecule inhibitors of Arp2/3 complex. *Nature*. 460: 1031–1034. <https://doi.org/10.1038/nature08231>
- Pelzer, D., L. de Plater, P. Bradbury, A. Eichmuller, A. Bourdais, G. Halet, and J.L. Maître. 2023. Cell fragmentation in mouse preimplantation embryos induced by ectopic activation of the polar body extrusion pathway. *EMBO J.*:e114415. <https://doi.org/10.1525/embj.2023114415>
- Piekny, A.J., and M. Glotzer. 2008. Anillin is a scaffold protein that links RhoA, actin, and myosin during cytokinesis. *Curr. Biol.* 18:30–36. <https://doi.org/10.1016/j.cub.2007.11.068>
- Pollard, T.D. 2007. Regulation of actin filament assembly by Arp2/3 complex and formins. *Annu. Rev. Biophys. Biomol. Struct.* 36:451–477. <https://doi.org/10.1146/annurev.biophys.35.040405.101936>
- Schatten, G., H. Schatten, I. Spector, C. Cline, N. Paweletz, C. Simerly, and C. Petzelt. 1986. Latrunculin inhibits the microfilament-mediated processes during fertilization, cleavage and early development in sea urchins and mice. *Exp. Cell Res.* 166:191–208. [https://doi.org/10.1016/0014-4827\(86\)90519-7](https://doi.org/10.1016/0014-4827(86)90519-7)
- Scheffler, K., J. Uraji, I. Jentoft, T. Cavazza, E. Mönnich, B. Mogessie, and M. Schuh. 2021. Two mechanisms drive pronuclear migration in mouse zygotes. *Nat. Commun.* 12:841. <https://doi.org/10.1038/s41467-021-21020-x>
- Sharif, B., T. Fadero, and A.S. Maddox. 2015. Anillin localization suggests distinct mechanisms of division plane specification in mouse oogenic meiosis I and II. *Gene Expr. Patterns*. 17:98–106. <https://doi.org/10.1016/j.gep.2015.03.002>
- Simerly, C., G. Nowak, P. de Lanerolle, and G. Schatten. 1998. Differential expression and functions of cortical myosin IIA and IIB isotypes during meiotic maturation, fertilization, and mitosis in mouse oocytes and embryos. *Mol. Biol. Cell*. 9:2509–2525. <https://doi.org/10.1091/mbc.9.9.2509>
- Swann, K. 1994. Ca^{2+} oscillations and sensitization of Ca^{2+} release in unfertilized mouse eggs injected with a sperm factor. *Cell Calcium*. 15: 331–339. [https://doi.org/10.1016/0143-4160\(94\)90072-8](https://doi.org/10.1016/0143-4160(94)90072-8)
- Tan, I., C.H. Ng, L. Lim, and T. Leung. 2001. Phosphorylation of a novel myosin binding subunit of protein phosphatase 1 reveals a conserved mechanism in the regulation of actin cytoskeleton. *J. Biol. Chem.* 276: 21209–21216. <https://doi.org/10.1074/jbc.M102615200>
- Tan, I., J. Yong, J.M. Dong, L. Lim, and T. Leung. 2008. A tripartite complex containing MRCK modulates lamellar actomyosin retrograde flow. *Cell*. 135:123–136. <https://doi.org/10.1016/j.cell.2008.09.018>
- Tan, I., J. Lai, J. Yong, S.F.Y. Li, and T. Leung. 2011. Chelerythrine perturbs lamellar actomyosin filaments by selective inhibition of myotonic dystrophy kinase-related Cdc42-binding kinase. *FEBS Lett.* 585:1260–1268. <https://doi.org/10.1016/j.febslet.2011.03.054>
- Tang, F., C. Barbacioru, Y. Wang, E. Nordman, C. Lee, N. Xu, X. Wang, J. Bodeau, B.B. Tuch, A. Siddiqui, et al. 2009. mRNA-Seq whole-transcriptome analysis of a single cell. *Nat. Methods*. 6:377–382. <https://doi.org/10.1038/meth.1315>
- Terada, Y., C. Simerly, and G. Schatten. 2000. Microfilament stabilization by jasplakinolide arrests oocyte maturation, cortical granule exocytosis, sperm incorporation cone resorption, and cell-cycle progression, but not DNA replication, during fertilization in mice. *Mol. Reprod. Dev.* 56: 89–98. [https://doi.org/10.1002/\(SICI\)1098-2795\(200005\)56:1<89::AID-MRD11>3.0.CO;2-1](https://doi.org/10.1002/(SICI)1098-2795(200005)56:1<89::AID-MRD11>3.0.CO;2-1)
- Unbekandt, M., and M.F. Olson. 2014. The actin-myosin regulatory MRCK kinases: Regulation, biological functions and associations with human cancer. *J. Mol. Med.* 92:217–225. <https://doi.org/10.1007/s00109-014-1133-6>
- Unbekandt, M., S. Belshaw, J. Bower, M. Clarke, J. Cordes, D. Crighton, D.R. Croft, M.J. Drysdale, M.J. Garnett, K. Gill, et al. 2018. Discovery of potent and selective MRCK inhibitors with therapeutic effect on skin cancer. *Cancer Res.* 78:2096–2114. <https://doi.org/10.1158/0008-5472.CAN-17-2870>
- Unbekandt, M., S. Lilla, S. Zanivan, and M.F. Olson. 2020. The CDC42 effector protein MRCK β autophosphorylates on Threonine 1108. *Small GTPases*. 11:451–460. <https://doi.org/10.1080/21541248.2018.1564472>
- Van Blervkom, J., and H. Bell. 1986. Regulation of development in the fully grown mouse oocyte: Chromosome-mediated temporal and spatial

- differentiation of the cytoplasm and plasma membrane. *J. Embryol. Exp. Morphol.* 93:213–238. <https://doi.org/10.1242/dev.93.1.213>
- Vaughan, E.M., A.L. Miller, H.Y.E. Yu, and W.M. Bement. 2011. Control of local Rho GTPase crosstalk by Abr. *Curr. Biol.* 21:270–277. <https://doi.org/10.1016/j.cub.2011.01.014>
- Vicente-Manzanares, M., X. Ma, R.S. Adelstein, and A.R. Horwitz. 2009. Non-muscle myosin II takes centre stage in cell adhesion and migration. *Nat. Rev. Mol. Cell Biol.* 10:778–790. <https://doi.org/10.1038/nrm2786>
- Vogt, E.J., K. Tokuhiro, M. Guo, R. Dale, G. Yang, S.W. Shin, M.J. Movilla, H. Shroff, and J. Dean. 2019. Anchoring cortical granules in the cortex ensures trafficking to the plasma membrane for post-fertilization exocytosis. *Nat. Commun.* 10:2271. <https://doi.org/10.1038/s41467-019-10171-7>
- Wang, Q., C. Racowsky, and M. Deng. 2011. Mechanism of the chromosome-induced polar body extrusion in mouse eggs. *Cell Div.* 6:17. <https://doi.org/10.1186/1747-1028-6-17>
- Wang, Z.B., Z.Z. Jiang, Q.H. Zhang, M.W. Hu, L. Huang, X.H. Ou, L. Guo, Y.C. Ouyang, Y. Hou, C. Brakebusch, et al. 2013. Specific deletion of Cdc42 does not affect meiotic spindle organization/migration and homologous chromosome segregation but disrupts polarity establishment and cytokinesis in mouse oocytes. *Mol. Biol. Cell.* 24:3832–3841. [https://doi.org/10.1091/mbe.e13-03-0123](https://doi.org/10.1091/mbc.e13-03-0123)
- Wang, H., Y. Li, J. Yang, X. Duan, P. Kalab, S.X. Sun, and R. Li. 2020. Symmetry breaking in hydrodynamic forces drives meiotic spindle rotation in mammalian oocytes. *Sci. Adv.* 6:eaaz5004. <https://doi.org/10.1126/sciadv.aaz5004>
- Wilkinson, S., H.F. Paterson, and C.J. Marshall. 2005. Cdc42-MRCK and Rho-ROCK signalling cooperate in myosin phosphorylation and cell invasion. *Nat. Cell Biol.* 7:255–261. <https://doi.org/10.1038/ncb1230>
- Yi, K., J.R. Unruh, M. Deng, B.D. Slaughter, B. Rubinstein, and R. Li. 2011. Dynamic maintenance of asymmetric meiotic spindle position through Arp2/3-complex-driven cytoplasmic streaming in mouse oocytes. *Nat. Cell Biol.* 13:1252–1258. <https://doi.org/10.1038/ncb2320>
- Yi, K., and R. Li. 2012. Actin cytoskeleton in cell polarity and asymmetric division during mouse oocyte maturation. *Cytoskeleton*. 69:727–737. <https://doi.org/10.1002/cm.21048>
- Yi, K., B. Rubinstein, and R. Li. 2013. Symmetry breaking and polarity establishment during mouse oocyte maturation. *Philos. Trans. R. Soc. Lond. B Biol. Sci.* 368:20130002. <https://doi.org/10.1098/rstb.2013.0002>
- Zhao, Z., and E. Manser. 2015. Myotonic dystrophy kinase-related Cdc42-binding kinases (MRCK), the ROCK-like effectors of Cdc42 and Rac1. *Small GTPases*. 6:81–88. <https://doi.org/10.1080/21541248.2014.1000699>
- Zhang, J., R. Ma, L. Li, L. Wang, X. Hou, L. Han, J. Ge, M. Li, and Q. Wang. 2017. Intersectin 2 controls actin cap formation and meiotic division in mouse oocytes through the Cdc42 pathway. *FASEB J.* 31:4277–4285. <https://doi.org/10.1096/fj.201700179R>
- Zhang, Y., J.C. Yu, T. Jiang, R. Fernandez-Gonzalez, and T.J.C. Harris. 2018. Collision of expanding actin caps with actomyosin borders for cortical bending and mitotic rounding in a syncytium. *Dev. Cell.* 45:551–564.e4. <https://doi.org/10.1016/j.devcel.2018.04.024>
- Zhong, Z.S., L.J. Huo, C.G. Liang, D.Y. Chen, and Q.Y. Sun. 2005. Small GTPase RhoA is required for ooplasmic segregation and spindle rotation, but not for spindle organization and chromosome separation during mouse oocyte maturation, fertilization, and early cleavage. *Mol. Reprod. Dev.* 71:256–261. <https://doi.org/10.1002/mrd.20253>
- Zhu, Z.Y., D.Y. Chen, J.S. Li, L. Lian, L. Lei, Z.M. Han, and Q.Y. Sun. 2003. Rotation of meiotic spindle is controlled by microfilaments in mouse oocytes. *Biol. Reprod.* 68:943–946. <https://doi.org/10.1095/biolreprod.102.009910>
- Zihni, C., E. Vlassaks, S. Terry, J. Carlton, T.K.C. Leung, M. Olson, F. Pichaud, M.S. Balda, and K. Matter. 2017. An apical MRCK-driven morphogenetic pathway controls epithelial polarity. *Nat. Cell Biol.* 19:1049–1060. <https://doi.org/10.1038/ncb3592>
- Zihni, C. 2021. MRCK: A master regulator of tissue remodeling or another ‘ROCK’ in the epithelial block? *Tissue Barriers*. 9:1916380. <https://doi.org/10.1080/21688370.2021.1916380>
- Zihni, C., A. Georgiadis, C.M. Ramsden, E. Sanchez-Heras, A.J. Haas, B. Nommiste, O. Semenyuk, J.W.B. Bainbridge, P.J. Coffey, A.J. Smith, et al. 2022. Spatiotemporal control of actomyosin contractility by MRCK β signaling drives phagocytosis. *J. Cell Biol.* 221:e202012042. <https://doi.org/10.1083/jcb.202012042>

Supplemental material

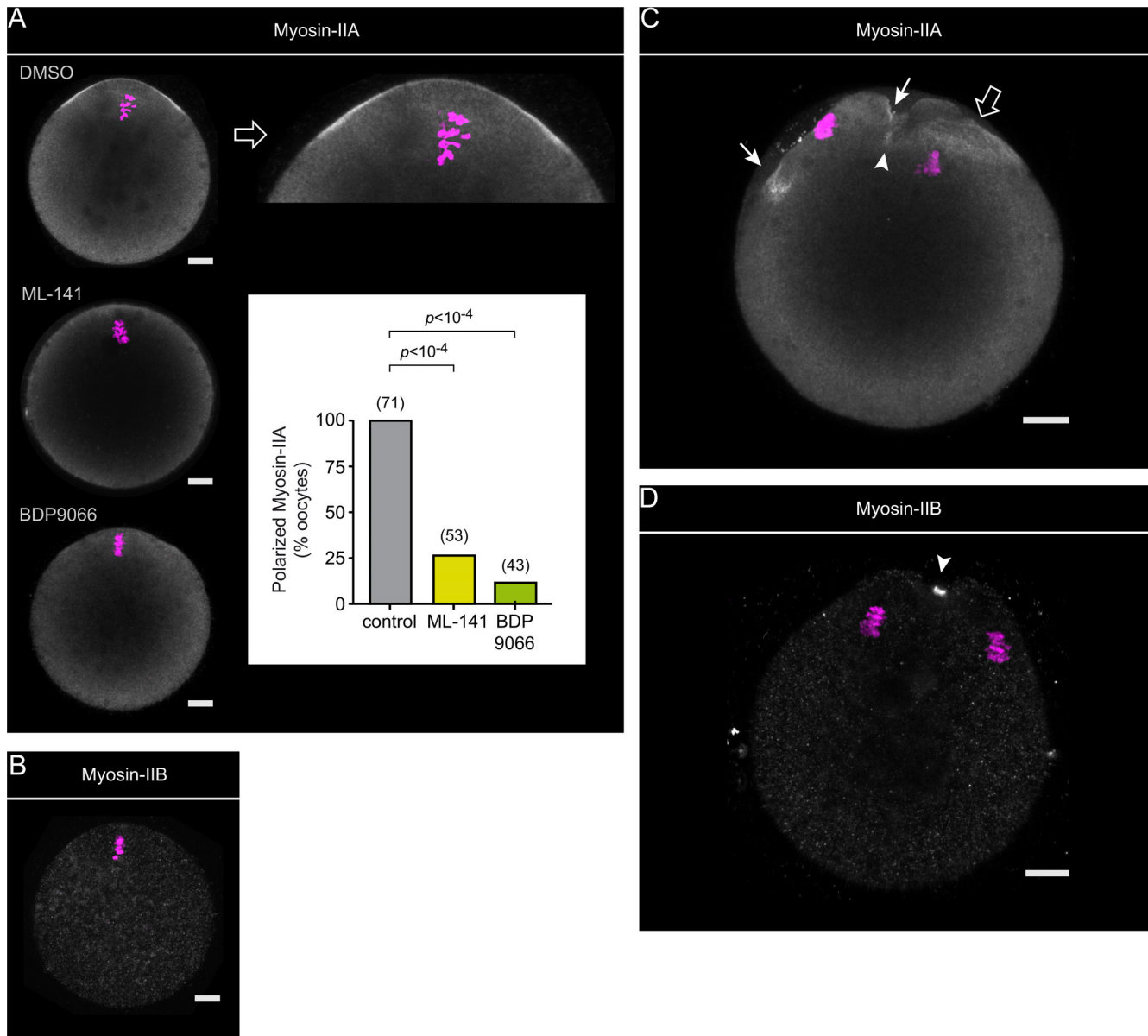


Figure S1. Myosin IIA and IIB heavy chain localization during MII and anaphase II. **(A)** Immunofluorescence detection of myosin IIA heavy chain in fixed MII oocytes treated with DMSO (top), ML-141 (5 μ M; middle), or BDP9066 (1 μ M; bottom). An enlarged view of the polarized cortex is shown for the control (DMSO) oocyte. The bar graph shows the fraction of oocytes (%) showing a polarized accumulation of myosin IIA under each experimental condition. P values were calculated using Fisher's exact test. The number of oocytes scored is indicated above each bar. **(B)** Immunofluorescence detection of myosin IIB heavy chain in a fixed MII oocyte. Note the absence of cortical localization. The image is representative of 44 similar observations. **(C)** Immunofluorescence detection of myosin IIA heavy chain in a fixed anaphase II oocyte that was activated with SrCl₂. The white arrows point to the myosin IIA ring in the nascent polar body. The heavy arrow points to myosin IIA reorganized into a cap above the internalized chromatid cluster. The white arrowhead points to myosin IIA in the cleavage furrow. **(D)** Immunofluorescence detection of myosin IIB heavy chain in a fixed anaphase II oocyte that was activated with SrCl₂. The white arrowhead points to myosin IIB concentrated in the cleavage furrow. Chromosomes were stained with TO-PRO-3 (magenta). Scale bars are 10 μ m.

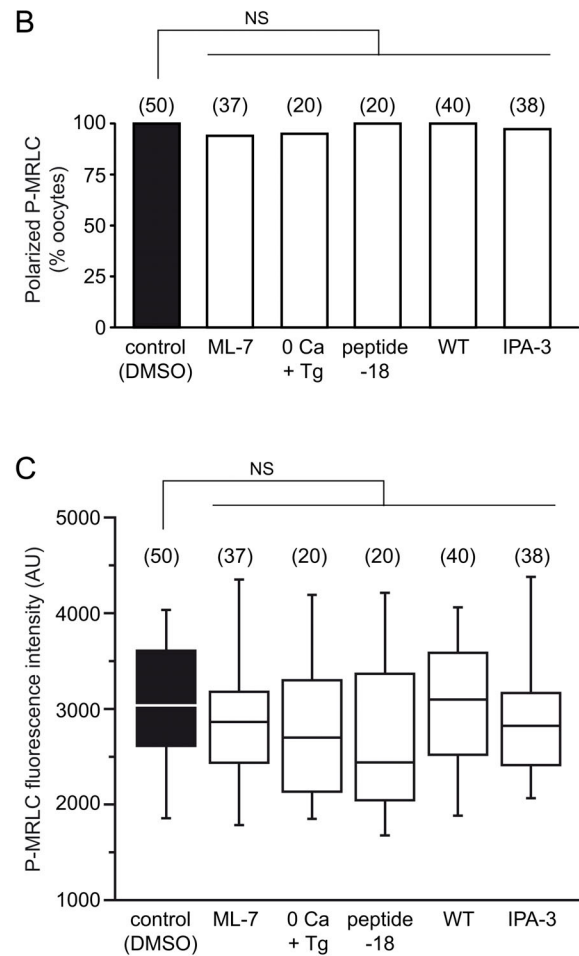
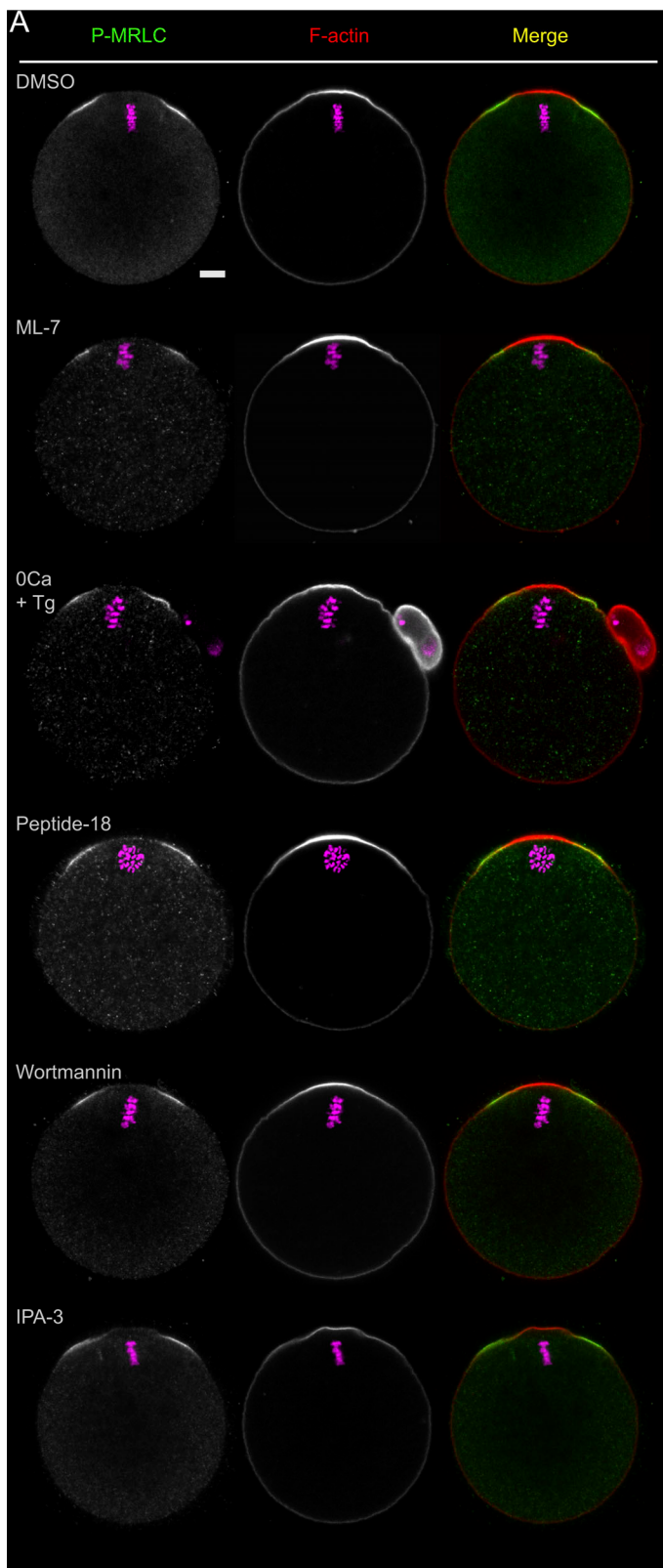


Figure S2. Ring myosin II activation is resistant to MLCK and PAK inhibitors. **(A)** Ring myosin II activation (P-MRLC) was monitored in MII oocytes after the following treatments (top to bottom): DMSO, ML-7 (15 μ M, 1 h), Ca^{2+} -free medium containing 1 mM EGTA and 10 μ M thapsigargin (0Ca + Tg; 1 h), peptide-18 microinjection followed by a 3-h culture, Wortmannin (1 μ M, 1 h), and IPA-3 (1 μ M, 1 h). F-actin was labeled with Alexa Fluor 568-phalloidin. Chromosomes were stained with TO-PRO-3 (magenta). The scale bar is 10 μ m and applies to the whole panel. **(B)** Bar graph illustrating the percentage of oocytes showing ring myosin II activation for each experimental condition. The number of oocytes scored is indicated above each bar. NS: not significant (Fisher's exact test). **(C)** Box plot showing the intensity of ring P-MRLC staining for the same populations of oocytes as shown in B. NS: not significant (two-tailed Student's t test).

AFull length MRCK β (human) : aa 1-1711**B**

	aa	polarized (n)
1-1711	1-1711	+(33/33)
1-1711**	1-1711**	-(0/43)
1015-1711	1015-1711	+(24/24)
1085-1711	1085-1711	+(21/21)
1229-1711	1229-1711	-(18/18)
1575-1711	1575-1711	-(0/26)
MCB-EGFP	1085-1618	+(26/26)
MCB(H1593/1596A)-EGFP	1085-1618**	-(0/25)

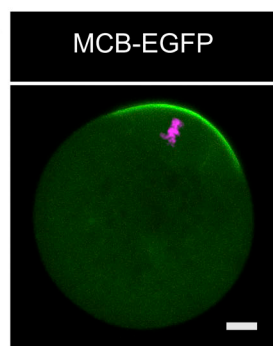
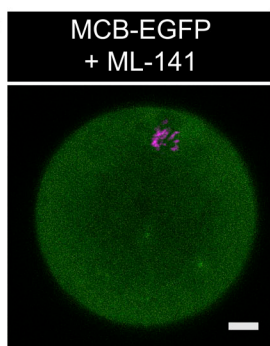
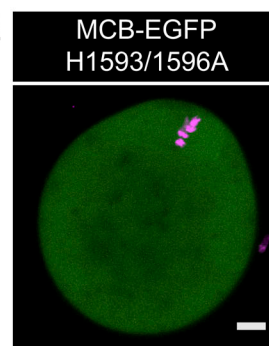
C**D****E**

Figure S3. Design of the Cdc42-GTP biosensor MCB-EGFP. **(A)** Schematic depicting the primary structure of full-length human MRCK β and its functional domains. C1: Protein kinase C conserved region 1. PH: Pleckstrin homology. CH: Citron homology. CRIB: Cdc42/Rac interactive binding. **(B)** Schematic outlining the different constructs generated through stepwise truncation to obtain a Cdc42-GTP biosensor, using full-length MRCK β -EGFP as a template. All constructs were expressed in MII oocytes via crRNA injection and examined for polarized localization in the cortex overlying maternal chromosomes. The total number of oocytes scored is indicated in parentheses for each construct, with an indication of cortical polarization (+) or absence of (-). While the CRIB domain alone was not sufficient for cortical localization, stepwise extensions toward the N-terminus allowed us to define a minimal Cdc42-GTP-binding fragment encompassing the PH, CH, and CRIB domains. This minimal fragment was used as a biosensor for Cdc42 activation, designated as MCB. Mutation of the two key histidine residues in the CRIB domain to alanine, corresponding to H1593/1596A in the full-length sequence, and indicated by double asterisks (**), abolished polarized localization. aa: Amino acids. **(C)** Confocal image of a live MII oocyte expressing the MCB-EGFP biosensor. **(D)** Confocal image of a live MII oocyte expressing the MCB-EGFP biosensor, and treated with ML-141 (5 μ M, 1 h). **(E)** Confocal image of a live MII oocyte expressing the MCB-EGFP biosensor bearing the H1593/1596A double substitution. Chromosomes were stained with SiR-DNA (magenta). Scale bars are 10 μ m.

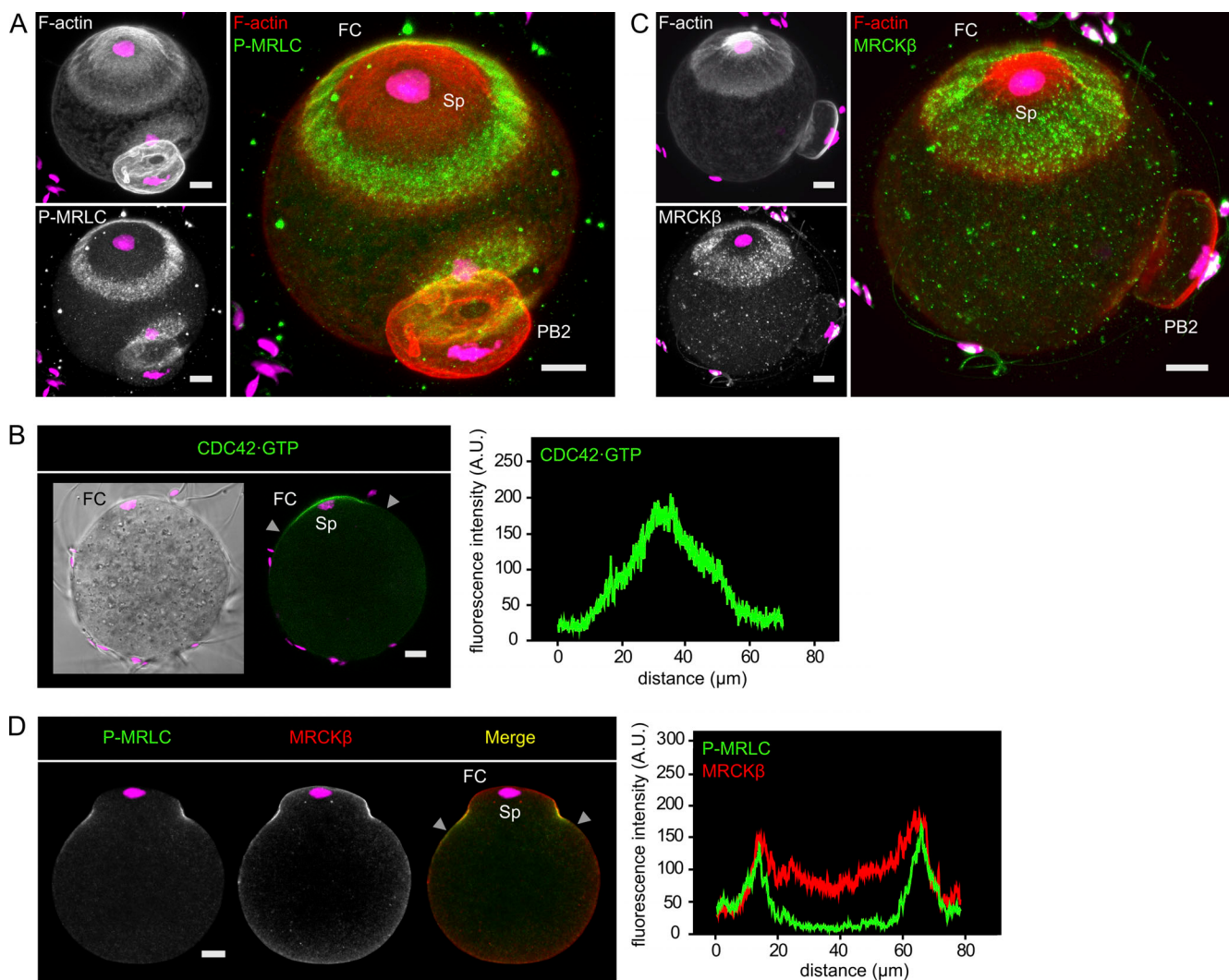


Figure S4. The Cdc42/MRCK/myosin II pathway is activated in the FC. **(A)** Immunofluorescence detection of activated myosin II (P-MRLC) in a fertilized oocyte. Images are z-compressions across the entire zygote volume, for 3D renditions, highlighting the FC. **(B)** Detection of Cdc42-GTP in the FC. The image shows a fertilized oocyte expressing the Cdc42-GTP biosensor MCB-EGFP. The oocyte was fertilized in vitro after zona pellucida removal. **(C)** Immunofluorescence detection of MRCK β in a fertilized oocyte. Images are z-compressions across the entire zygote volume, for 3D renditions, highlighting the FC. **(D)** Immunofluorescence detection of activated myosin II (P-MRLC) and MRCK β in a fertilized oocyte. Fluorescence intensity profiles in B and D correspond to the cortical regions delineated by the gray arrowheads in the merge images. F-actin was labeled with Alexa Fluor 568-phalloidin. Chromosomes were stained with TO-PRO-3 (magenta). Sp: sperm chromatin. Scale bars are 10 μ m.

Video 1. Live imaging of a MII oocyte treated with BDP9066 (2 μ M). Time-lapse recording was started at the time of drug addition. Images were acquired every 2 min. Yellow lines indicate the position of the polarized cortex and the opposite cortex at the start of recording. Chromosomes were stained with Si-RNA.

Video 2. Live imaging of anaphase II in a control oocyte treated with DMSO. The oocyte was injected with cRNAs encoding EGFP-MAP4 to label microtubules (green) and H2B-mCherry to label chromosomes (magenta). Images were acquired every 2 min.

Video 3. Live imaging of anaphase II in an oocyte treated with BDP9066, showing the spindle distortion phenotype. The oocyte was injected with cRNAs encoding EGFP-MAP4 to label microtubules (green) and H2B-mCherry to label chromosomes (magenta). Images were acquired every 2 min.

Video 4. **Live imaging of anaphase II in an oocyte treated with BDP9066, showing the spindle breakage phenotype.** The oocyte was injected with cRNAs encoding EGFP-MAP4 to label microtubules (green) and H2B-mCherry to label chromosomes (magenta). Images were acquired every 2 min.

Video 5. **Confocal z-stack across an SrCl₂-activated oocyte expressing MRCK β -K105A, showing the spindle breakage phenotype.** The oocyte was stained for tubulin (green), F-actin (red), and chromatin (magenta). Images on the left show an overlay of the spindle, chromosome, and brightfield channels.